All-sky search for short gravitational-wave bursts in the second Advanced LIGO and Advanced Virgo run

B. P. Abbott *et al.*[*]

(LIGO Scientific Collaboration and Virgo Collaboration)

We present the results of a search for short-duration gravitational-wave transients in the data from the second observing run of Advanced LIGO and Advanced Virgo. We search for gravitational-wave transients with a duration of milliseconds to approximately one second in the 32–4096 Hz frequency band with minimal assumptions about the signal properties, thus targeting a wide variety of sources. We also perform a matched-filter search for gravitational-wave transients from cosmic string cusps for which the waveform is well modeled. The unmodeled search detected gravitational waves from several binary black hole mergers which have been identified by previous analyses. No other significant events have been found by either the unmodeled search or the cosmic string search. We thus present the search sensitivities for a variety of signal waveforms and report upper limits on the source rate density as a function of the characteristic frequency of the signal. These upper limits are a factor of 3 lower than the first observing run, with a 50% detection probability for gravitational-wave emissions with energies of $\sim 10^{-9}$ $M_\odot c^2$ at 153 Hz. For the search dedicated to cosmic string cusps we consider several loop distribution models, and present updated constraints from the same search done in the first observing run.

I. INTRODUCTION

The Advanced LIGO and Advanced Virgo detectors [1,2] have completed their second observing run (O2) which lasted from November 30, 2016 to August 25, 2017. During O2, gravitational waves (GWs) were detected from seven binary black hole (BBH) mergers [3], as well as the first binary neutron star merger ever observed [4]. While binary systems of compact objects such as black holes and/ or neutron stars are a main source of short-duration transient GWs observable by LIGO and Virgo, there are other predicted sources of GW transients. Some examples include core-collapse supernovae [5], pulsar glitches [6], neutron stars collapsing into black holes [7], and cosmic string cusps [8–10]. There also exists the possibility of new, as-of-yet unpredicted GW sources.

In order to maximize our ability to detect any such GWs, there exist a variety of so-called all-sky searches—those with no prior assumption on the time of arrival of the GW signal or its location in the sky. These searches fall broadly into two categories: searches that target GWs from specific sources, and those that look for GWs using minimal assumptions about the source or signal morphology. Targeted analyses include searches for merging stellar-mass binary black holes and neutron stars [3] as well as intermediate-mass black holes [11], and searches for cosmic string signals [12–14]. The more generic analyses look for both long-duration GW transients [15–17] and short-duration events [18–20]. In this paper, we report on the results of two all-sky searches. The first is a generic search for short-duration GW transients. The second is a targeted search for cosmic string signals using the matched-filtering method with template waveforms predicted from past theoretical studies [8–10].

The rest of this paper is organized as follows. In Sec. II we review the data set used for these analyses. Section III is dedicated to the search for unmodeled GW transients and is divided into three parts. First, in Sec. III A, we describe the three search algorithms used to look for generic unmodeled GW transients and the results of those searches. Second, in Sec. III B we discuss briefly some aspects regarding the detection of the known BBH signals. In Sec. III C, we discuss the sensitivity of these searches and give rate-density limits of transient GW events, excluding known compact binary sources. Section IV is dedicated to the modeled cosmic string cusps search. We briefly outline the search algorithm used for the analysis, and present our results and updated parameter constraints. Finally, in Sec. V, we discuss the results and implications from both the unmodeled GW transients search and the modeled cosmic string cusp search.

II. O2: THE SECOND ADVANCED-DETECTOR OBSERVING RUN

Our data set ranges from November 30, 2016 to August 25, 2017. Prior to August 2017, only the Hanford and

---

[*]Deceased.

Livingston Advanced LIGO detectors were in observational mode. On August 1, 2017, Advanced Virgo joined the detector network. During O2, the combined Hanford-Livingston network sensitivity was slightly more sensitive than it was in the first observing run (O1), achieving a roughly 30% increase in the binary-neutron-star (BNS) range [21]. The Advanced Virgo detector was less sensitive than the Advanced LIGO detectors, with a BNS range that was roughly a factor of 2–3 lower [21]. As a result of this, including the Virgo data set did not improve the sensitivity to the short-duration searches presented in this paper. We thus present the analysis of only the Hanford-Livingston data.

Over the course of O2, the live time of the data collected by the two LIGO detectors was about 158 days for Hanford, and about 154 days for Livingston. The amount of coincident data between the two detectors is approximately 118 days. Not all of this data is ultimately analyzed though, as the data can sometimes be polluted by instrumental and environmental noise artifacts. In particular, transient noise events known as "glitches" can potentially mimic GW properties thereby lowering the sensitivity of searches for short-duration GW bursts. To mitigate the effect of instrumental and environmental noise, a large number of auxiliary channels within the interferometer are monitored in order to characterize the relation between artifacts in these channels and the GW strain channel. This auxiliary channel information is used to identify periods of poor data quality, which is then excluded from the analysis [22–25]. The calibration uncertainties in O2 data for Hanford and Livingston respectively are 2.6% and 3.9% in amplitude, and 2.4 and 2.2 degrees in phase [26,27]. Additionally, for the first time in Advanced LIGO data, methods to subtract some well-identified sources of noise from the data are used, increasing Hanford's sensitivity by 10% [28]. While these methods remove many known artifacts, not all glitches are removed. Thus, the pipelines in this paper have been designed to confidently distinguish between real GW signals and instrumental glitches.

The data used is this paper is part of the O1 Data Release and O2 Data Release through the Gravitational Wave Open Science Center [29], and can be found at Ref. [30].

III. UNMODELED GW TRANSIENTS

We describe here the unmodeled search for short-duration transient signals. Given the uncertainty and the wide spectrum of expected signals, the algorithms are designed to use minimal assumptions on the expected waveform and consider signals with a duration of a few seconds or less in the frequency range of 32 to 4096 Hz. This covers a wide parameter space of sources, including GWs from mergers of compact objects such as neutron stars or black holes. While there exist more narrowly focused searches that target GWs from compact binary systems which are naturally more sensitive to this type of

signal [31–33], the unmodeled searches presented here are sensitive to a wider variety of potential sources. In this work, we identify and then remove the known BBH sources in our analysis results, in order to focus on searching for previously unidentified transients.

We use the same three unmodeled analyses that were used in the O1 search [20]. By using multiple pipelines we have the ability to independently verify search results. Additionally, the regions of parameter space where these algorithms are the most sensitive is not the same for every pipeline, and so the combination of the different approaches increases our ability to detect a wide range of signals. Below we describe the three different algorithms used to search for transient GW events.

A. Searches

1. Coherent WaveBurst

Coherent WaveBurst (cWB) is an algorithm based on the maximum-likelihood-ratio statistic applied to power excesses in the time-frequency domain [34]. This analysis is done by using a wavelet transform at various resolutions, as to adapt the time-frequency characterization to the signal features. cWB has been used in the previous LIGO-Virgo searches for transient signals [18–20].

The cWB analysis is split into two frequency bands: low and high frequency. The triggers are further divided into search bins, similar to how it was done for the O1 analysis.

The low-frequency analysis covers the parameter space ranging from 32–1024 Hz, and performs a down sampling of the data. The triggers are divided into two different bins. The first bin, $LF1$, is polluted by nonstationary power-spectrum lines and a class of low-frequency, short-duration glitches known as "blip" glitches for which there is no specific data quality veto [22]. These are selected using the same criteria described in Ref. [23]: nonstationary lines localize more than 80% of their energy in a frequency bandwidth of less than 5 Hz; blip glitches are identified according to their waveform properties so that their quality factor (Q) is less than 3. The second bin, $LF2$ contains the remaining low-frequency triggers. In the O1 analysis [20] there was a third class focusing on events with morphology similar to compact object binaries—specifically events that chirped up in frequency. This class is not considered in this work, since the results for a cWB dedicated search for chirping signals was reported in Ref. [3]. The search in Ref. [3] differs from the one presented here in both post-production thresholds and selection of power excesses in time-frequency. The latter was performed in Ref. [3] favoring time-frequency patterns with increasing frequency over time. This feature, in addition to dedicated thresholds, reduces the background and increases the sensitivity to compact binary coalescence waveforms.

The high-frequency analysis uses data in the 1024–4096 Hz range and is also divided into two bins. The first

bin, *HF*1, contains triggers with central frequencies above 2048 Hz, and events with central frequencies in the band 1000–1150 Hz for the period of the run before Jan 22, 2017. The second bin, *HF*2, contains the remaining triggers. The change in the bin definition pre– and post– Jan 22nd is due to an excess of glitches that were occurring around 1100 Hz between October 2016 and January 2017. These glitches were identified as originating from length fluctuations in the Hanford detector's output mode cleaner optical cavity, and were successfully mitigated for the remainder of O2 [35].

Periods of poor data quality were removed as described in previous searches for short-duration GW events [19,20,36]. There is some additional loss of live time in analyzable data because cWB requires at least 1200 seconds of coincident data per analyzable segment. The final amount of data analyzed by cWB was 113.9 days.

The cWB analysis is performed by dividing the run into reduced periods of consecutive time epochs (called "chunks"). Each chunk is composed of about 5 days of live time, resulting in 21 chunks in total. The background distribution of triggers for each individual chunk is calculated by time shifting the data of one detector with respect to the other detector by an amount that breaks any correlation between detectors for a real signal. Each chunk was time shifted to give about 500 years of background data, which allows the search to reach the statistical significance of 1/100 years while allowing for a trial factor of 2 for each of the low- and high-frequency bands. Performing the analyses in chunks takes into account fluctuating noise levels of the detectors over the duration of the observing run.

The significance of each trigger found in the real coincident data is then calculated by comparing the coherent network signal-to-noise ratio (SNR) η_c [20] with the background distribution of the chunk to which it belongs.

The search results for the cWB low- and high-frequency bands are shown in Fig. 1. In the low-frequency search band, cWB found six of the known BBH events with inverse false-alarm rates (iFARs) ranging from 290 years for GW170814 to 0.07 years for GW170729. The loudest trigger in the high-frequency search band has an iFAR of 7 years, and it is related to some disturbances appearing around 1600 Hz. To search for new events, we remove all previously known GW signals. In this case, this means removing the six BBH signals identified by the search. The remaining events, shown as dashed curves in Fig. 1, are all consistent with expected noise events.

2. Omicron-LIB

Omicron-LIB (oLIB) is a hierarchical search algorithm. oLIB first analyzes the data streams of individual detectors, referred to as an incoherent analysis. It then follows up stretches of data that are potentially correlated across the
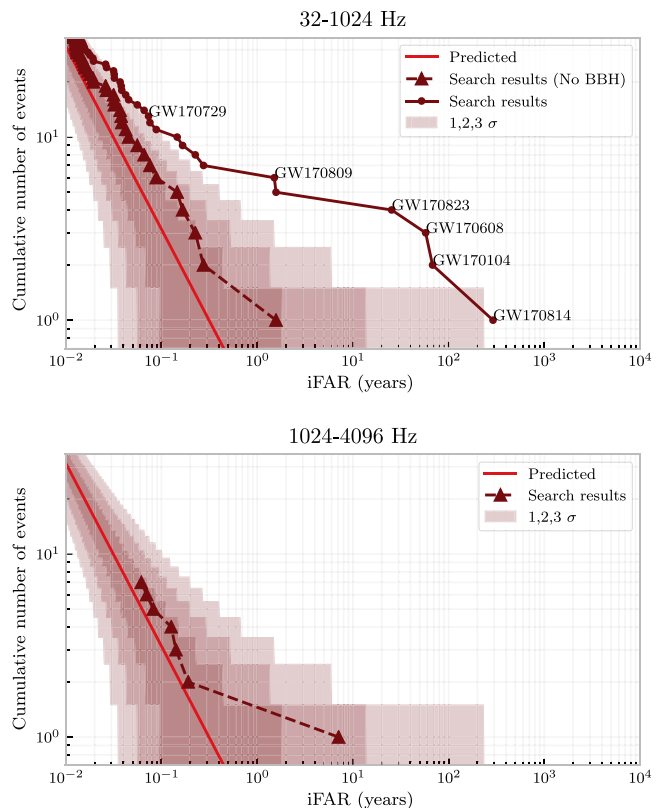

FIG. 1. Cumulative number of events versus inverse false-alarm rate found by the cWB search using all O2 data (circle points) and the cWB search where times around all compact binary coalescence sources (see Table I from Ref. [3]) have been dropped out (triangular points). The solid line shows the expected background, given the analysis time. The shaded regions show the 1, 2, and 3σ Poisson uncertainty regions. Top: Search results from the cWB low-frequency (32–1024 Hz) band, with results grouped considering all the bins, applying a trials factor equal to 2. Bottom: Search results from the cWB high-frequency (1024–4096 Hz) band. No triggers associated with known BBH signals were found in this search.

detector network, referred to as a coherent analysis. The incoherent analysis ("Omicron") [37] flags stretches of coincident excess power. The coherent follow-up ("LIB") [38] models GW signals and noise transients with a single sine-Gaussian, and then produces two different Bayes factors. Each of these Bayes factors is expressed as the natural logarithm of the evidence ratio of two hypotheses: 1) a GW signal versus Gaussian noise (BSN) and 2) a coherent GW signal versus incoherent noise transients (BCI). The joint likelihood ratio of these two Bayes factors, Λ, is used as a ranking statistic to assign a significance to each event.

For this analysis, oLIB analyzes two frequency bands: a low-frequency search band covering 32–1024 Hz, and a high-frequency search band covering 1024–2048 Hz. Similarly to how the analysis was done in O1, low-frequency oLIB event candidates are divided by the quality

factor of the signal into high-Q and low-Q search bins (see Ref. [20]). These bins are defined by slightly different cuts than in O1, with the exact choices being made after the background data is analyzed and prior to the analysis of real coincident data. The low-Q bin contains only events whose median quality factor $\tilde{Q}$ lies within the range of 0.2–1.2 and whose median frequency f_0 lies within the range of 32–1024 Hz. The high-Q bin contains only events whose $\tilde{Q}$ lies within the range 2–108 and whose f_0 lies within the range of 120–1024 Hz. The Q range of 1.2–2 is excluded from the analysis *a priori* as that region of parameter space is known to be populated by the blip glitches. The high-frequency search band contains only events whose $\tilde{Q}$ lies within the range of 2–108 and whose f_0 lies within the range of 1124–2048 Hz. The lower frequency cutoff here is set to 1124 Hz in order to reject a high number of glitches in the 1024–1124 Hz frequency range which were described in Sec. III A 1. In all bins, event candidates are also required to have positive Bayes factors, meaning the GW signal model is favored over the noise models. A trials factor of 2 is applied to the low-frequency search to account for the independent bins.

Two improvements are made to the O2 oLIB search, as compared to the O1 search that increase the sensitivity. The first is that log BSN is used as a search statistic instead of BSN, which improves the accuracy of oLIB's kernel-density estimates of the signal and noise likelihoods. Second, event candidates are required to have nonextreme SNR balance across the detector network. Specifically, we require event candidates to satisfy $\max\{BSN_{H1}/BSN_{L1}, BSN_{L1}/BSN_{H1}\} < 9$, where BSN_i is the BSN Bayes factor estimated using only the data of detector i. This cut helps mitigate the contamination of coincident non-Gaussian noise transients, which tend to have much larger SNR imbalance than GW signals.

After removing the periods of poor data quality, oLIB analyzed 114.7 days of coincident detector live time. This is slightly more than what was analyzed by cWB because oLIB does not have the same requirement of 1200 seconds of continuous data. Using the time-slide method, oLIB collected 496 years worth of data to determine the background distribution of glitches. The significance of triggers found in the zero-lag data is calculated by comparing oLIB's ranking statistic to that of the background distribution. Similar to the O1 analysis, we select single-detector events with SNR > 5.0. The search results are shown in Fig. 2. No coincident events satisfy the cuts of the low-Q bin, and the event rate of the high-frequency search matches the expected rate of accidental noise coincidences. Two events in the high-Q bin are previously identified BBH events (GW170823 and GW170104). Again, to search for previously unidentified GW events, the previously known events are removed. The results after removing these events are shown as the dashed lines in Fig. 2. We notice a small deviation of the high-Q bin's event rate from the expected
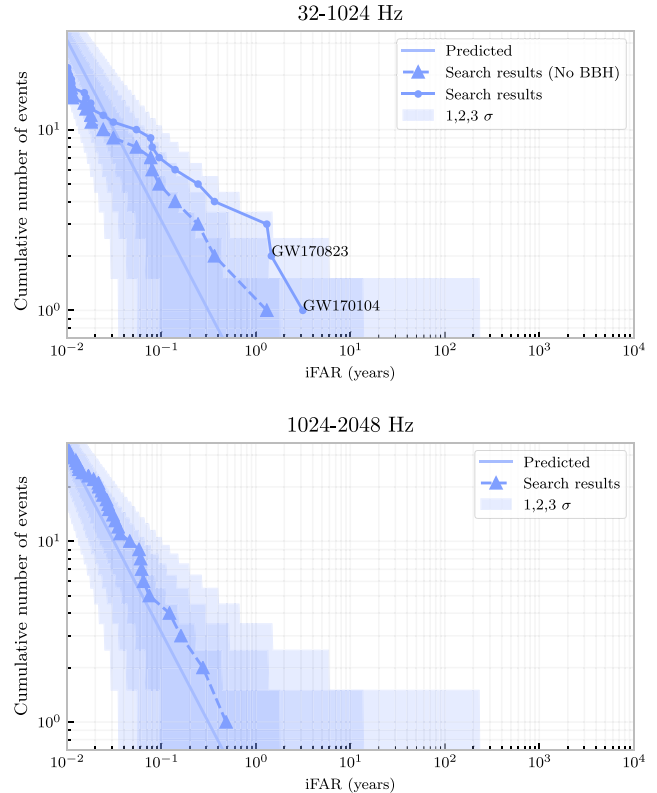

FIG. 2. Cumulative number of events versus inverse false-alarm rate found by the oLIB search using all O2 data (circle points) and the oLIB search where times around all compact binary coalescence sources (see Table I from Ref. [3]) have been dropped out (triangular points). The solid line shows the expected background, given the analysis time. The shaded regions show the 1, 2, and 3σ Poisson uncertainty regions. Top: The results of the low-frequency (32–1024 Hz) band. The low-frequency band contains two search bins—a high-Q bin and a low-Q bin—but as there were no foreground triggers in the low-Q bin, only the high-Q bin is represented here. Bottom: The search results for the high-frequency (1024–2048) band, which contains only a single search bin.

noise rate for the loudest event candidates, even after all known BBH events are excised from the analysis. After applying the trials factor of 2, the iFAR of our loudest event candidate is about 1.4 years, which corresponds to a p-value of 0.22. Using a five-threshold Event Stacking Test [39], the deviation peaks in significance at the fifth-loudest event, and the overall p-value of the test is 0.17. Both of these p-values correspond to one-sided outliers that are less than 1σ in units of Gaussian standard deviations, and neither signifies a confident detection of GWs. Thus, we conclude that the oLIB search did not find any new GW events.

3. BayesWave follow-up

The BayesWave (BW) algorithm [40,41] models non-Gaussian features in GW detector data as the sum of

sine-Gaussian wavelets using a reversible jump Markov chain Monte Carlo (RJMCMC), where the number of wavelets used is not fixed *a priori* but determined via the RJMCMC. BayesWave reconstructs the data in two different models: the signal model which treats the data in each interferometer as Gaussian noise plus a common astrophysical signal, and the glitch model which treats the data as Gaussian noise plus independent transient noise artifacts in each detector. BayesWave then calculates the natural log of the Bayesian evidence of each model.

The detection statistic used is the log signal-to-glitch Bayes factor ($\ln \mathcal{B}_{sg}$), which is the difference between the logarithm of the two evidences. A negative $\ln \mathcal{B}_{sg}$ indicates more evidence for a glitch, and a positive $\ln \mathcal{B}_{sg}$ indicates more evidence for a signal. Beyond minor improvements to the algorithm, the most notable change to BayesWave's mode of operation between O1 and O2 is the prior on the number of wavelets (N_w) used in the reconstruction. While O1 used a flat distribution of $N_w \in [0, 20]$ [40], for O2 a prior based on the posterior distribution of N_w during O1 was implemented into the code. To construct the prior we used the *maximum a posteriori* number of wavelets from a sample of significant background events from O1 to infer the distribution of wavelet dimension. This histogram was then fit to a ratio of polynomials to predict the density at model sizes larger than the O1 cutoff of $N_w = 20$. This prior peaks at $N_w = 3$, and falls off for higher numbers of wavelets.

In both O1 and O2 BayesWave was used as a follow-up to the cWB pipeline, as adding this follow-up has been shown to enhance confidence in GW detections [42]. For O2, BayesWave followed up cWB events in the low-frequency search, treating the $LF1$ and $LF2$ search bins as a single bin, and using a threshold of $\eta_c = 9$. BayesWave used the same approach used by cWB to divide the 113.9 days of analyzable data into chunks of approximately 5 days, and used the same background data set from time slides.

There were nine cWB triggers which were above the η_c threshold, five of which are known BBH signals.[1] The results of the BayesWave analysis is shown in Fig. 3. The five BBH events were the most significant triggers in the BayesWave results, and after removing them as we did for the cWB and oLIB analysis, all events are consistent with accidental noise fluctuations.

B. Known BBH signals

The LIGO and Virgo Collaboration recently released the First GW Transient Catalog (GWTC-1) [3], which reports all GWs detected by searches targeting compact binary signals in O1 and O2. GWTC-1 includes ten signals from BBH mergers, seven of which occurred during O2. These

---

[1]The only known BBH signal detected by the cWB all-sky algorithm that did not pass the η_c threshold was GW170729.
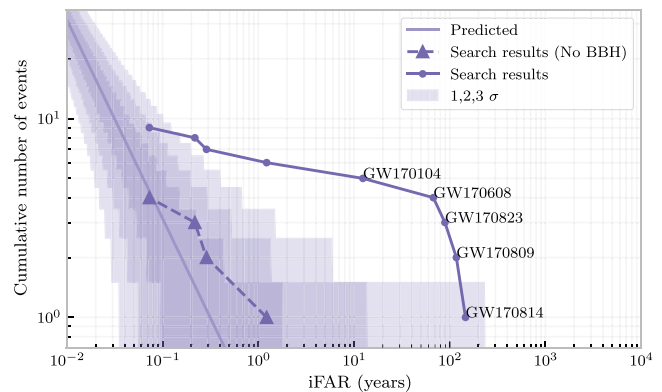

FIG. 3. Cumulative number of events versus inverse false-alarm rate found by the BW follow-up to the cWB low-frequency search using all O2 data (circle points) and the BW follow-up where times around all compact binary coalescence sources (see Table I from Ref. [3]) have been dropped out (triangular points). The solid line shows the expected background, given the analysis time. The shaded regions show the 1, 2, and 3σ Poisson uncertainty regions.

BBHs tend to be short-duration signals that are within the parameter space covered by the unmodeled searches presented here. So while this search does not target BBH signals, we still found a number of previously identified BBH signals.

Of the seven BBH events in O2, six were identified by at least one of the generic transient search algorithms. cWB identified six of the BBH events found in O2. Of those six, five were above the threshold used by the BW follow-up. After applying the selection cuts described above, oLIB identifies two of the BBH events: GW170104 and GW170823. Two other BBH signals, GW170814 and GW170608, are both excluded from the oLIB analysis as a result of narrowly missing some of the data-quality cuts chosen *a priori* for the analysis, but both become clear detections if they are manually added back into the analysis. One BBH event, GW170818, was not detected by any of the unmodeled pipelines. The matched-filter search in Ref. [3] that identified GW170818 found it only had an SNR of 4.1 in the Hanford detector. As the unmodeled analyses are less sensitive to quieter signals like this one, it was missed by this search.

Two cases worth mentioning are GW170729 and GW170809. GW170729 has a lower iFAR than the one given in GWTC-1 [3] (50 years). This is expected since, as already explained in Sec. III A 1, the cWB results reported in GWTC-1 are from a version of cWB with settings for a dedicated search for compact binary coalescence. GW170809 instead was not found by cWB in GWTC-1 because that particular time-frequency selection included noise excesses. This decreases the coherence of this event between the detectors, which means it did not pass one of the post-production thresholds and thus was not assigned any significance.

There was also one binary neutron star merger (GW170817) detected in O2 [4]. This was a longer signal than the BBH events, appearing in the LIGO data for almost 30 seconds. The unmodeled pipelines presented here search for signals with a duration of about one second or less, and so did not detect GW170817.

We defer discussion of the astrophysical properties and implications of these events to GWTC-1. For the remainder of this paper, we excise known BBH events from our results and place upper limits on event rates from sources that have not been previously identified by targeted search pipelines.

C. Sensitivity

We measure the detection efficiency of the searches for unmodeled transient events by adding simulated GW signals into real detector data, and using the unmodeled analyses described in Sec. III A to search for these injected signals. In this work, we use as a detection threshold an iFAR of 100 years.

We do not have accurate waveforms for many of the potential sources in the parameter space of the unmodeled analyses described here. However, a variety of waveform morphologies can be used to approximate physical situations that are likely to be generated by astrophysical systems. We use these waveforms, distributed through a wide range of amplitudes, durations, and characteristic frequencies to test our unmodeled searches.

1. Injection data set

The set of injected signals used in this analysis includes sine-Gaussian (SG), Gaussian (GA), and white-noise burst (WNB) waveforms. These waveforms, which are not derived from any particular astrophysical model, are the standard in the testing and development of searches for unmodeled GW signals [19,20]. Each of these injected waveforms can be described by a few characteristic parameters: SG waveforms are parametrized by their central frequency (f_0) and quality factor (Q); GA waveforms are parametrized by the duration (τ); and finally WNB waveforms are parametrized by their bandwidth (Δf), lower frequency bound (f_{low}), and duration in time (τ). Details about the specifics of these waveforms can be found in Ref. [19]. To fully test the pipelines' sensitivity to the range of signals, these waveforms are injected with a range of amplitudes, which we measure as the root-mean-square strain (h_{rss}) of the waveform at Earth.

The injected signal set for this work was produced using MINKE [43], an open-source PYTHON package developed during the O1 detector run. It produces data that contains simulated transient GW signals using the signal generation provided by LALSIMULATION routines as a part of the LIGO Algorithm Library [44].

For the signal set used in this analysis, signals were produced at a rate of once every 50 seconds. These were spaced evenly throughout the total time of the run, although the center time of each signal is shifted by a time drawn from a uniform distribution, between -5 s and $+5$ s from each division of the time span. The h_{rss} of each signal was drawn from the distribution $r + 50/r$, which is uniform in the square of the signal distance r^2, constructed such that the minimum h_{rss} produced was 5×10^{-23} and the maximum was 1×10^{-20}.

Signals are produced for each of the detectors, with the sky location chosen by drawing from a uniform distribution across the sky, and a uniform distribution over waveform polarization; the waveform's sky location is used to calculate the injection time for each signal for each detector. The remaining parameters of each waveform are held fixed for each injection set.

2. Results

Table I shows the specific parameters of all the waveforms analyzed here, and the h_{rss} value at which 50% of the injections are detected by each pipeline for each signal morphology. The O2 search is more sensitive than in O1. This increase in efficiency can be attributed to both the increase in detector sensitivity and the improvements made to the algorithms to better deal with instrumental noise.

The introduction of analysis in chunks, for instance, allows for adapting the threshold to the level of nearby background noise. Moreover, cWB is now using two search

TABLE I.   The h_{rss} values, in units of 10^{-22} Hz$^{-1/2}$, at which 50% detection efficiency is achieved at a FAR of 1 in 100 yr for each of the algorithms, as a function of the injected signal morphologies. "N/A" denotes that 50% detection efficiency was not achieved. "$\cdots$" denotes the waveform was not analyzed by oLIB and BW because its characteristic frequency did not meet the search cuts.

Morphology	cWB	oLIB	BW
Gaussian pulses			
$\tau = 0.1$ ms	8.4	6.2	N/A
$\tau = 2.5$ ms	11	5.3	N/A
sine-Gaussian wavelets			
$f_0 = 70$ Hz, $Q = 3$	4.9	$\cdots$	N/A
$f_0 = 70$ Hz, $Q = 100$	6.4	$\cdots$	N/A
$f_0 = 153$ Hz, $Q = 8.9$	1.4	1.3	16
$f_0 = 235$ Hz, $Q = 100$	3.3	1.1	1.4
$f_0 = 554$ Hz, $Q = 8.9$	1.8	1.5	N/A
$f_0 = 849$ Hz, $Q = 3$	5.5	2.0	17
$f_0 = 1304$ Hz, $Q = 9$	3.3	2.8	$\cdots$
$f_0 = 1615$ Hz, $Q = 100$	3.6	3.3	$\cdots$
$f_0 = 2000$ Hz, $Q = 3$	5.4	5.3	$\cdots$
$f_0 = 2477$ Hz, $Q = 8.9$	7.5	$\cdots$	$\cdots$
$f_0 = 3067$ Hz, $Q = 3$	9.7	$\cdots$	$\cdots$
White-Noise Bursts			
$f_{low} = 100$ Hz, $\Delta f = 100$ Hz, $\tau = 0.1$ s	1.4	3.0	3.0
$f_{low} = 250$ Hz, $\Delta f = 100$ Hz, $\tau = 0.1$ s	1.4	3.8	3.8
$f_0 = 750$ Hz, $\Delta f = 100$ Hz, $\tau = 0.1$ s	1.8	3.7	4.2

bins instead of three. Consequently the threshold value applied to η_c decreases at the same FAR. The combination of the two effects leads to significant improvements in the efficiency for waveforms belonging to the $LF1$ bin with respect to O1 results.

oLIB cuts and tunings are especially beneficial for the GA and WNB waveforms, as oLIB now achieves 50% detection efficiency for all of these waveform morphologies, which it did not achieve in O1. Nevertheless, these additional cuts do hurt the detection efficiency in some regions of parameter space, such as the band below 120 Hz in the high-Q bin. For example, the detection efficiency of the SG waveform at 70 Hz is exactly 0 (although oLIB's detection efficiency for this morphology was also negligible in O1 due to its long ~1.5 s duration).

The BayesWave follow-up is the least sensitive to SG signals, as shown in Ref. [42]. BayesWave's detection statistic, $\ln \mathcal{B}_{sg}$ scales linearly with the number of sine-Gaussian basis functions used in the signal reconstruction, meaning for simple signals that can be accurately represented with a single sine-Gaussian it is harder to distinguish between the signal and glitch models [45]. For signals with more complicated structure in time-frequency space (such as BBH signals which increase in frequency over time), BayesWave is more efficient at distinguishing between the signal and glitch models. Since the SG and GA waveforms used here can be accurately modeled as single sine-Gaussian wavelets, BayesWave is less sensitive to these signals. One improvement made between O1 and O2 is the addition of a jump proposal in the MCMC that helped with the mixing of higher Q signals. This resulted in an increased sensitivity to higher Q signals.

From the detection efficiencies given in Table I, we can make a statement on the minimum amount of energy that needs to be emitted by a GW in order to be detected. To do this, we assume a standard candle source at a distance of $r_0 = 10$ kpc radiating GWs at a central frequency of f_0. The amount of energy radiated is then [19]

$$E_{\mathrm{GW}} = \frac{\pi^2 c^3}{G} r_0^2 f_0^2 h_0^2. \qquad (1)$$

We use the h_{rss} values of 50% detection efficiency given in Table I to find the minimum amount of energy that needs to be radiated by the GW source in order to be detected by at least one of the unmodeled searches. These results are shown in Fig. 4, along with the results from the O1 unmodeled all-sky search [20] for comparison.

Given that the searches did not find any additional detection results for GW sources beyond the known BBH signals, we can update the upper limit of the rate per unit volume of non-BBH standard-candle sources [19,20], shown in Fig. 4. For these upper limits, we use the SG and WNB injection sets listed in Table I as representative morphologies of non-BBH GW bursts.
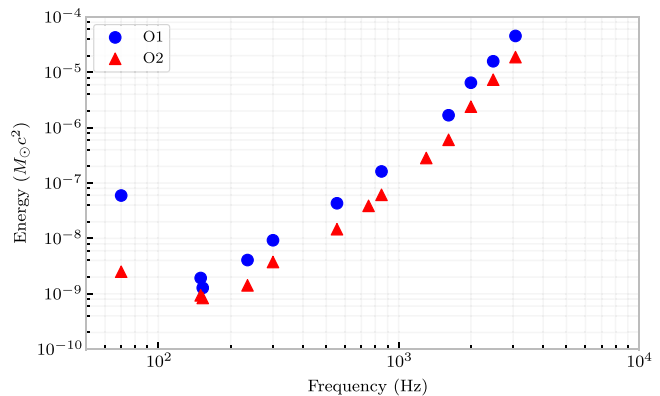

FIG. 4. The GW emitted energy in units of solar masses that correspond to a 50% detection efficiency at an iFAR of 100 years, for a source emitting at 10 kpc. The waveforms represented here include all of the sine-Gaussian and white-noise burst injections as give in Table I. We present the best sensitivity achieved by any of the unmodeled search pipelines, for both the O1 [20] and O2 searches.

The markers represent the upper limit at 90% confidence for the rate density [19], calculated assuming that no noise events meet the detection threshold in our analysis data. The results shown in Fig. 5 assume that 1 $M_\odot c^2$ of GW energy has been emitted from the source, but the upper limits can be scaled to any emission energy E_{GW} by using Eq. (1) to find that the rate density scales $\propto E_{\mathrm{GW}}^{-\frac{3}{2}}$.

Compared to the rate-density upper limits placed in O1 [20] using only the cWB analysis on SG injections, the upper limits reported here for the O2 run are at least a factor
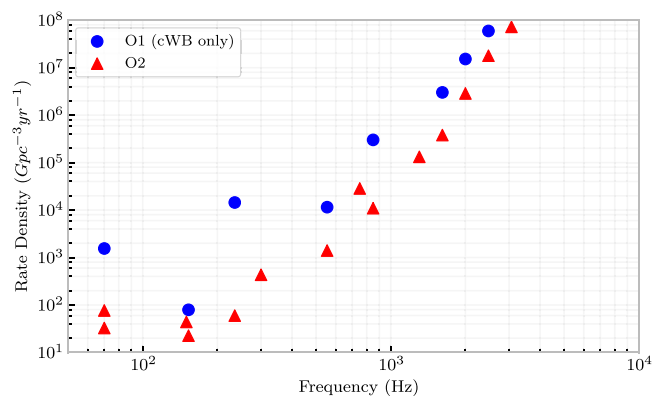

FIG. 5. Upper limits on the 90% confidence intervals for the GW rate density, as measured in O2 using the SG and WNB waveforms listed in Table I. Here we show the strictest upper limit achieved by any of the three unmodeled search pipelines. These results can be scaled to any emission energy E_{GW} using the rate density $\propto E_{\mathrm{GW}}^{-3/2}$. We also show the results from the O1 all-sky search [20], which presented results from the cWB pipeline for sine-Gaussian waveforms. Note that the O1 cWB search used three bins, which mostly affected the efficiency for waveforms belonging to $LF1$ (i.e., 70 and 235 Hz, shown here as blue dots).

of 3 stricter than the O1 upper limits, with much greater improvements at certain frequencies. We would expect these upper limits to be at least a factor of 2.4 stricter than the O1 upper limits based on the fact that the pipelines are analyzing a factor of 2.4 more live time than in the O1 search. The greatest improvements in the upper limits between O1 and O2 are due to the fact that here we present the strictest upper limit from any of the three algorithms described here, as opposed to the O1 results which only reported the cWB limits. Because cWB is not necessarily the pipeline with the greatest sensitivity for every frequency, we get substantial improvement from considering results from all pipelines.

The rest of the improvement can be attributed to the more sensitive Hanford-Livingston detector network, and improvements made to the analysis algorithms. These upper limits are almost 2 orders of magnitude stricter than those set in all of the initial-detector observing runs (i.e., S5 and S6) at a lower iFAR detection threshold of 8 years.

IV. COSMIC STRING CUSPS

Cosmic strings [46] are one-dimensional topological defects thought to be the relics of phase transitions in the early Universe. When a cosmic string interacts with another string at two points or with itself, it intercommutes and forms a loop. Cosmic string loops oscillate and form cusps, which are points along the loop with large Lorentz boosts. Cusps are expected to produce powerful bursts of GWs, having distinct signatures. In particular, the waveform is well predicted by theory [8–10], which offers the possibility to specifically search for these signals in GW data. Here, we report on a template-based analysis designed to search for GW signals from cosmic string cusps in LIGO and Virgo data. In this work we will focus on Nambu-Goto strings [47] whose thickness is approximated to be zero, and assume the intercommutation probability equals unity.

A. The search

The cosmic string cusp waveform in the frequency domain is given by $h_{\mathrm{cusp}}(f) = Af^{-4/3}$, where A and f are the signal amplitude and frequency respectively [8–10]. The signal spectrum is limited by a high-frequency cutoff determined by the angle between the beamed emission from the cusp and the observer. This parameter is unknown such that a bank of waveform templates, with different high-frequency cutoff values, is used to perform a matched-filter analysis.

We present the results of the search using the O2 data for GW bursts from cosmic string cusps. This search was conducted in the past using initial LIGO-Virgo data [13] and Advanced LIGO O1 data [14], and no signal was found. Here, we have used the same analysis methods, which we describe briefly below.

GW bursts from cosmic string cusps are searched by projecting the data onto the bank of templates. Triggered events detected at the Hanford and Livingston detectors are then set in time coincidence in order to reject single-detector noise. Then a multivariate likelihood ratio [48] Λ is computed for each of the surviving events, and is used to rank the coincident events.

The pipeline's sensitivity to cosmic string signals was estimated by injecting simulated cusp signals of different amplitudes into the data, and checking whether they were recovered by the pipeline. The sensitivity as a function of amplitude can be used to set constraints on cosmic string parameters, if no signals with high significance are found. To maximize the sensitivity to GW signals we performed data quality studies to reject glitches that may mimic the waveform from cosmic string cusps. We have considered all data quality flags and vetoes produced for transient gravitational-wave searches [19,22]. For each chunk, we look at the effectiveness of the data quality flags which is defined to be the ratio of the fraction of glitches removed to the fraction of analyzable lifetime removed by the veto. We select those for which that ratio is greater than 2. The search sensitivity was slightly improved by using a selection of data quality flags.

B. Results

The cumulative event rate as a function of the ranking statistic Λ is displayed in the upper plot of Fig. 6. The highest-ranked event is measured with $\Lambda_h \simeq 9.01$. The ranking value of this event does not deviate significantly from the background distribution estimated by performing the analysis over 6000 time-shifted data sets, made by shifting the Livingston data a sufficient amount so that the events surviving the coincidence check will only be noise. Therefore, we cannot claim this event to be the result of a GW signal produced by cosmic strings. Although we cannot rule out the possibility that the highest-ranked events are real signals, data quality studies find that these events are consistent with blip glitches, the time-frequency structure of which matches very well the waveform of a cusp signal. The exact cause of these glitches is unknown.

The lower plot in Fig. 6 shows the detection efficiency of cusp events as a function of the injected signal amplitude A. The efficiency is computed as the fraction of simulated signals recovered with $\Lambda > \Lambda_h$. Here we show the sensitivity curve combining O1 and O2 data, as the sensitivity of the O2 LIGO cusp search is comparable to the O1 LIGO one [14].

We also conducted a three-detector search using the data collected by Advanced Virgo in August 2017, corresponding to ~17 days of data. The search false-alarm rate improved, in combination with a significant reduction of coincident blip noise signals. However the sensitivity of the Advanced Virgo detector was not sufficient to improve the
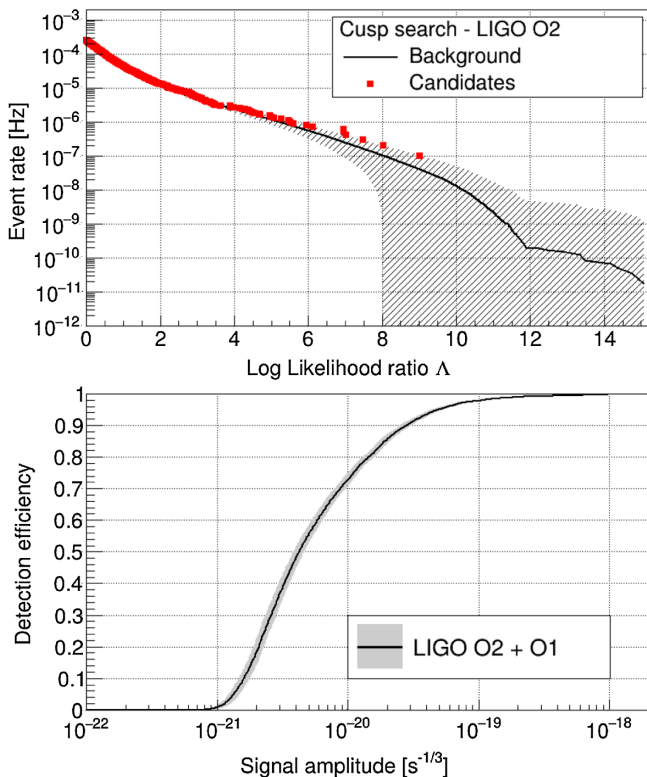
FIG. 6. Top: Cumulative event rate for the cosmic string search as a function of the ranking statistic Λ (red points). The black line shows the expected background distribution with a $\pm 1\sigma$ statistical error represented by the hatched area. The highest-ranked event ($\Lambda_h \simeq 9.01$) is consistent with the background. Bottom: Search detection efficiency as a function of the cusp signal amplitude, when combining O1 and O2 LIGO data sets. This is measured by the fraction of simulated cusp events recovered with $\Lambda > \Lambda_h$.

detection efficiency of cosmic string signals and so here we only present results using Hanford and Livingston data.

Using the O1 and O2 combined detection efficiency, we place constraints on the string tension $G\mu$ ($c = 1$), where G is Newton's constant and μ is the mass per unit length. This is achieved by comparing the experimental sensitivity to cosmic string signals with predicted detection rates. The expected rate can be derived from cosmic string loop distribution models relying on numerical simulations of cosmic string networks. We examine two analytic models of cosmic string loop distributions already used in the O1 analysis. The loop density modeled in Ref. [49] was first considered. However, the sensitivity to burst signals produced by such loops is not sufficient to constrain $G\mu$ significantly. We tested another loop density modeled in Ref. [50], where tiny loops are produced in greater amount than in Ref. [49], producing a higher rate of GW bursts. In this case, the upper limit on the string tension is $G\mu \leq 4.2 \times 10^{-10}$, with a 95% confidence level. This O1 + O2 upper limit has improved by a factor ~ 2 with respect to the previous limit obtained with O1 data alone.

Under the assumption of these loop distributions, our nondetection is consistent with the nondetection of the stochastic background created by these bursts, from which stronger constraints on $G\mu$ are obtained [51].

V. CONCLUSION

This paper reports the results for two searches for short-duration GWs in the second observing run: one for generic unmodeled GW transient signals and the other focused on modeled cosmic string cusps.

The most generic search for unmodeled GW transients uses minimal assumptions on the signal waveform, direction or arrival time and is performed using three different methods. Apart from the known BBH signals described in detail in Ref. [3], no other signals were found by the unmodeled search. We used our null detection to pose rate-density upper limits on short-duration transient GW events not associated with BBH systems. These limits are stricter than the limits derived from the O1 analysis by a factor of at least 3, owing to a combination of better detector sensitivities, increased observation time, and algorithmic developments.

In the search for modeled cosmic string cusps, we selected two analytic models for loop distributions already used in the O1 analysis [14]. We improved the constraints on the string tension $G\mu$ for the model that produces a large amount of small loops [50]. Our results are complemented by the O2 stochastic results [51], which have obtained tighter constraints on the string tension $G\mu$.

LIGO and Virgo began their next observing run in April 2019. In addition to the detectors already in operation, two new ground-based detectors will join the search for GWs in the future. KAGRA, in Japan, has just finished installation and is aiming to join the O3 run, and LIGO-India is currently under construction [21]. Improved sensitivities and additional detectors will lead to better sensitivities for short-duration GW searches in the future.

[1] J. Aasi *et al.* (LIGO Scientific Collaboration), Advanced LIGO, Classical Quantum Gravity **32**, 115012 (2015).

[2] F. Acernese *et al.* (Virgo Collaboration), Advanced Virgo: A second-generation interferometric gravitational wave detector, Classical Quantum Gravity **32**, 024001 (2015).

[3] B. P. Abbott *et al.* (LIGO Scientific and Virgo Collaborations), GWTC-1: A gravitational-wave transient catalog of compact binary mergers observed by LIGO and Virgo during the first and second observing runs, arXiv: 1811.12907.

[4] B. P. Abbott *et al.* (LIGO Scientific and Virgo Collaborations), GW170817: Observation of Gravitational Waves from a Binary Neutron Star Inspiral, Phys. Rev. Lett. **119**, 161101 (2017).

[5] C. L. Fryer and K. C. B. New, Gravitational waves from gravitational collapse, Living Rev. Relativity **14**, 1 (2011).

[6] N. Andersson and G. L. Comer, Probing Neutron-Star Superfluidity with Gravitational-Wave Data, Phys. Rev. Lett. **87**, 241101 (2001).

[7] L. Baiotti, I. Hawke, and L. Rezzolla, On the gravitational radiation from the collapse of neutron stars to rotating black holes, Classical Quantum Gravity **24**, S187 (2007).

[8] T. Damour and A. Vilenkin, Gravitational Wave Bursts from Cosmic Strings, Phys. Rev. Lett. **85**, 3761 (2000).

[9] T. Damour and A. Vilenkin, Gravitational wave bursts from cusps and kinks on cosmic strings, Phys. Rev. D **64**, 064008 (2001).

[10] T. Damour and A. Vilenkin, Gravitational radiation from cosmic (super)strings: Bursts, stochastic background, and observational windows, Phys. Rev. D **71**, 063510 (2005).

[11] B. P. Abbott *et al.* (LIGO Scientific and Virgo Collaborations), Search for intermediate mass black hole binaries in the first observing run of Advanced LIGO, Phys. Rev. D **96**, 022001 (2017).

[12] B. P. Abbott *et al.* (LIGO Scientific Collaboration), First LIGO search for gravitational wave bursts from cosmic (super)strings, Phys. Rev. D **80**, 062002 (2009).

[13] J. Aasi *et al.* (LIGO Scientific and Virgo Collaborations), Constraints on Cosmic Strings from the LIGO-Virgo Gravitational-Wave Detectors, Phys. Rev. Lett. **112**, 131101 (2014).

[14] B. P. Abbott *et al.* (LIGO Scientific and Virgo Collaborations), Constraints on cosmic strings using data from the first Advanced LIGO observing run, Phys. Rev. D **97**, 102002 (2018).

[15] B. P. Abbott *et al.* (LIGO Scientific and Virgo Collaborations), An all-sky search for long-duration gravitational wave transients with LIGO, Phys. Rev. D **93**, 042005 (2016).

[16] B. P. Abbott *et al.* (LIGO Scientific and Virgo Collaborations), All-sky search for long-duration gravitational wave transients in the first Advanced LIGO observing run, Classical Quantum Gravity **35**, 065009 (2018).

[17] B. P. Abbott *et al.* (LIGO Scientific and Virgo Collaborations), All-sky search for long-duration gravitational-wave transients in the second Advanced LIGO observing run, Phys. Rev. D **99**, 104033 (2019).

[18] J. Abadie *et al.* (LIGO Scientific and Virgo Collaborations), All-sky search for gravitational-wave bursts in the first joint LIGO-GEO-Virgo run, Phys. Rev. D **81**, 102001 (2010).

[19] J. Abadie *et al.* (LIGO Scientific and Virgo Collaborations), All-sky search for gravitational-wave bursts in the second joint LIGO-Virgo run, Phys. Rev. D **85**, 122007 (2012).

[20] B. P. Abbott *et al.* (LIGO Scientific and Virgo Collaborations), All-sky search for short gravitational-wave bursts in the first advanced ligo run, Phys. Rev. D **95,** 042003 (2017).

[21] B. P. Abbott *et al.* (LIGO Scientific and Virgo Collaborations), Prospects for observing and localizing gravitational-wave transients with Advanced LIGO, Advanced Virgo and KAGRAs, Living Rev. Relativity **21,** 3 (2018).

[22] B. P. Abbott *et al.* (LIGO Scientific and Virgo Collaborations), Characterization of transient noise in Advanced LIGO relevant to gravitational wave signal GW150914, Classical Quantum Gravity **33,** 134001 (2016).

[23] B. P. Abbott *et al.* (LIGO Scientific and Virgo Collaborations), Observing gravitational-wave transient GW150914 with minimal assumptions, Phys. Rev. D **93,** 122004 (2016); Publisher's Note, Phys. Rev. D **94,** 069903(A) (2016).

[24] B. P. Abbott *et al.* (LIGO Scientific and Virgo Collaborations), Effects of data quality vetoes on a search for compact binary coalescences in Advanced LIGO first observing run, Classical Quantum Gravity **35,** 065010 (2018).

[25] L. K. Nuttall, Characterizing transient noise in the LIGO detectors, Phil. Trans. R. Soc. A **376,** 20170286 (2018).

[26] A. D. Viets, M. Wade, A. L. Urban, S. Kandhasamy, J. Betzwieser, D. A. Brown, J. Burguet-Castell, C. Cahillane, E. Goetz, K. Izumi, S. Karki, J. S. Kissel, G. Mendell, R. L. Savage, X. Siemens, D. Tuyenbayev, and A. J. Weinstein, Reconstructing the calibrated strain signal in the advanced LIGO detectors, Classical Quantum Gravity **35,** 095015 (2018).

[27] C. Cahillane, J. Betzwieser, D. A. Brown, E. Goetz, E. D. Hall, K. Izumi, S. Kandhasamy, S. Karki, J. S. Kissel, G. Mendell, R. L. Savage, D. Tuyenbayev, A. Urban, A. Viets, M. Wade, and A. J. Weinstein, Calibration uncertainty for advanced ligo's first and second observing runs, Phys. Rev. D **96,** 102001 (2017).

[28] J. C. Driggers *et al.* (LIGO Scientific Collaboration), Improving astrophysical parameter estimation via offline noise subtraction for Advanced LIGO, Phys. Rev. D **99,** 042001 (2019).

[29] M. Vallisneri, J. Kanner, R. Williams, A. Weinstein, and B. Stephens, The LIGO open science center, J. Phys. Conf. Ser. **610,** 012021 (2015).

[30] LIGO Scientific and Virgo Collaborations, LIGO Virgo strain data from observing run O2 (Nov 2016-Aug 2017) (2019), https://www.gw-openscience.org/O2/.

[31] S. A. Usman *et al.*, The PyCBC search for gravitational waves from compact binary coalescence, Classical Quantum Gravity **33,** 215004 (2016).

[32] A. Nitz *et al.*, Pycbc: O2 production release 9, free software (2017), https://github.com/gwastro/pycbc/tree/v1.6.8.

[33] C. Messick, Analysis framework for the prompt discovery of compact binary mergers in gravitational-wave data, Phys. Rev. D **95,** 042001 (2017).

[34] S. Klimenko, G. Vedovato, M. Drago, F. Salemi, V. Tiwari, G. A. Prodi, C. Lazzaro, S. Tiwari, F. Da Silva, and G. Mitselmakher, Method for detection and reconstruction of gravitational wave transients with networks of advanced detectors, Phys. Rev. D **93,** 042004 (2016).

[35] https://alog.ligo-wa.caltech.edu/aLOG/index.php?callRep= 33104.

[36] B. P. Abbott *et al.* (LIGO Scientific Collaboration), Search for gravitational-wave bursts in the first year of the fifth LIGO science run, Phys. Rev. D **80,** 102001 (2009).

[37] F. Robinet, Omicron: An algorithm to detect and characterize transient noise in gravitational-wave detectors (2015), https://tds.ego-gw.it/ql/?c=10651.

[38] R. Lynch, S. Vitale, R. Essick, E. Katsavounidis, and F. Robinet, Information-theoretic approach to the gravitational-wave burst detection problem, Phys. Rev. D **95,** 104046 (2017).

[39] R. Lynch, S. Vitale, and E. Katsavounidis, Beyond single-threshold searches: The event stacking test, arXiv:1811.01297.

[40] N. J. Cornish and T. B. Littenberg, BayesWave: Bayesian inference for gravitational wave bursts and instrument glitches, Classical Quantum Gravity **32,** 135012 (2015).

[41] https://git.ligo.org/lscsoft/bayeswave.

[42] J. B. Kanner, T. B. Littenberg, N. Cornish, M. Millhouse, E. Xhakaj, F. Salemi, M. Drago, G. Vedovato, and S. Klimenko, Leveraging waveform complexity for confident detection of gravitational waves, Phys. Rev. D **93,** 022002 (2016).

[43] D. Williams, Minke, free software (2018), https://doi.org/10.5281/zenodo.1699336.

[44] LIGO Scientific Collaboration, LIGO Algorithm Library—LALSuite, free software (GPL) (2018) https://git.ligo.org/lscsoft/lalsuite.

[45] T. B. Littenberg, J. B. Kanner, N. J. Cornish, and M. Millhouse, Enabling high confidence detections of gravitational-wave bursts, Phys. Rev. D **94,** 044050 (2016).

[46] A. Vilenkin and E. Shellard, *Cosmic Strings and Other Topological Defects* (Cambridge University Press, Cambridge, England, 2000).

[47] T. Goto, Relativistic quantum mechanics of one-dimensional mechanical continuum and subsidiary condition of dual resonance model, Prog. Theor. Phys. **46,** 1560 (1971).

[48] K. C. Cannon, A Bayesian coincidence test for noise rejection in a gravitational-wave burst search, Classical Quantum Gravity **25,** 105024 (2008).

[49] J. J. Blanco-Pillado, K. D. Olum, and B. Shlaer, The number of cosmic string loops, Phys. Rev. D **89,** 023512 (2014).

[50] C. Ringeval, M. Sakellariadou, and F. Bouchet, Cosmological evolution of cosmic string loops, J. Cosmol. Astropart. Phys. 02 (2007) 023.

[51] B. P. Abbott *et al.* (LIGO Scientific and Virgo Collaborations), A search for the isotropic stochastic background using data from Advanced LIGO's second observing run, arXiv:1903.02886.

B. P. Abbott,[1] R. Abbott,[1] T. D. Abbott,[2] S. Abraham,[3] F. Acernese,[4,5] K. Ackley,[6] C. Adams,[7] R. X. Adhikari,[1] V. B. Adya,[8] C. Affeldt,[9,10] M. Agathos,[11,12] K. Agatsuma,[13] N. Aggarwal,[14] O. D. Aguiar,[15] L. Aiello,[16,17] A. Ain,[3] P. Ajith,[18] G. Allen,[19]

A. Allocca,[20,21] M. A. Aloy,[22] P. A. Altin,[8] A. Amato,[23] S. Anand,[1] A. Ananyeva,[1] S. B. Anderson,[1] W. G. Anderson,[24] S. V. Angelova,[25] S. Antier,[26] S. Appert,[1] K. Arai,[1] M. C. Araya,[1] J. S. Areeda,[27] M. Arène,[26] N. Arnaud,[28,29] S. M. Aronson,[30] S. Ascenzi,[16,31] G. Ashton,[6] S. M. Aston,[7] P. Astone,[32] F. Aubin,[33] P. Aufmuth,[10] K. AultONeal,[34] C. Austin,[2] V. Avendano,[35] A. Avila-Alvarez,[27] S. Babak,[26] P. Bacon,[26] F. Badaracco,[16,17] M. K. M. Bader,[36] S. Bae,[37] J. Baird,[26] P. T. Baker,[38] F. Baldaccini,[39,40] G. Ballardin,[29] S. W. Ballmer,[41] A. Bals,[34] S. Banagiri,[42] J. C. Barayoga,[1] C. Barbieri,[43,44] S. E. Barclay,[45] B. C. Barish,[1] D. Barker,[46] K. Barkett,[47] S. Barnum,[14] F. Barone,[48,5] B. Barr,[45] L. Barsotti,[14] M. Barsuglia,[26] D. Barta,[49] J. Bartlett,[46] I. Bartos,[30] R. Bassiri,[50] A. Basti,[20,21] M. Bawaj,[51,40] J. C. Bayley,[45] M. Bazzan,[52,53] B. Bécsy,[54] M. Bejger,[26,55] I. Belahcene,[28] A. S. Bell,[45] D. Beniwal,[56] M. G. Benjamin,[34] B. K. Berger,[50] G. Bergmann,[9,10] S. Bernuzzi,[11] C. P. L. Berry,[57] D. Bersanetti,[58] A. Bertolini,[36] J. Betzwieser,[7] R. Bhandare,[59] J. Bidler,[27] E. Biggs,[24] I. A. Bilenko,[60] S. A. Bilgili,[38] G. Billingsley,[1] R. Birney,[25] O. Birnholtz,[61] S. Biscans,[1,14] M. Bischi,[62,63] S. Biscoveanu,[14] A. Bisht,[10] M. Bitossi,[29,21] M. A. Bizouard,[64] J. K. Blackburn,[1] J. Blackman,[47] C. D. Blair,[7] D. G. Blair,[65] R. M. Blair,[46] S. Bloemen,[66] F. Bobba,[67,68] N. Bode,[9,10] M. Boer,[64] Y. Boetzel,[69] G. Bogaert,[64] F. Bondu,[70] R. Bonnand,[33] P. Booker,[9,10] B. A. Boom,[36] R. Bork,[1] V. Boschi,[29] S. Bose,[3] V. Bossilkov,[65] J. Bosveld,[65] Y. Bouffanais,[52,53] A. Bozzi,[29] C. Bradaschia,[21] P. R. Brady,[24] A. Bramley,[7] M. Branchesi,[16,17] J. E. Brau,[71] M. Breschi,[11] T. Briant,[72] J. H. Briggs,[45] F. Brighenti,[62,63] A. Brillet,[64] M. Brinkmann,[9,10] P. Brockill,[24] A. F. Brooks,[1] J. Brooks,[29] D. D. Brown,[56] S. Brunett,[1] A. Buikema,[14] T. Bulik,[73] H. J. Bulten,[74,36] A. Buonanno,[75,76] D. Buskulic,[33] C. Buy,[26] R. L. Byer,[50] M. Cabero,[9,10] L. Cadonati,[77] G. Cagnoli,[78] C. Cahillane,[1] J. Calderón Bustillo,[6] T. A. Callister,[1] E. Calloni,[79,5] J. B. Camp,[80] W. A. Campbell,[6] M. Canepa,[81,58] K. C. Cannon,[82] H. Cao,[56] J. Cao,[83] G. Carapella,[67,68] F. Carbognani,[29] S. Caride,[84] M. F. Carney,[57] G. Carullo,[20,21] J. Casanueva Diaz,[21] C. Casentini,[85,31] S. Caudill,[36] M. Cavaglià,[86,87] F. Cavalier,[28] R. Cavalieri,[29] G. Cella,[21] P. Cerdá-Durán,[22] E. Cesarini,[88,31] O. Chaibi,[64] K. Chakravarti,[3] S. J. Chamberlin,[89] M. Chan,[45] S. Chao,[90] P. Charlton,[91] E. A. Chase,[57] E. Chassande-Mottin,[26] D. Chatterjee,[24] M. Chaturvedi,[59] K. Chatziioannou,[92] B. D. Cheeseboro,[38] H. Y. Chen,[93] X. Chen,[65] Y. Chen,[47] H.-P. Cheng,[30] C. K. Cheong,[94] H. Y. Chia,[30] F. Chiadini,[95,68] A. Chincarini,[58] A. Chiummo,[29] G. Cho,[96] H. S. Cho,[97] M. Cho,[76] N. Christensen,[98,64] Q. Chu,[65] S. Chua,[72] K. W. Chung,[94] S. Chung,[65] G. Ciani,[52,53] M. Cieślar,[55] A. A. Ciobanu,[56] R. Ciolfi,[99,53] F. Cipriano,[64] A. Cirone,[81,58] F. Clara,[46] J. A. Clark,[77] P. Clearwater,[100] F. Cleva,[64] E. Coccia,[16,17] P.-F. Cohadon,[72] D. Cohen,[28] M. Colleoni,[101] C. G. Collette,[102] C. Collins,[13] M. Colpi,[43,44] L. R. Cominsky,[103] M. Constancio Jr.,[15] L. Conti,[53] S. J. Cooper,[13] P. Corban,[7] T. R. Corbitt,[2] I. Cordero-Carrión,[104] S. Corezzi,[39,40] K. R. Corley,[105] N. Cornish,[54] D. Corre,[28] A. Corsi,[84] S. Cortese,[29] C. A. Costa,[15] R. Cotesta,[75] M. W. Coughlin,[1] S. B. Coughlin,[106,57] J.-P. Coulon,[64] S. T. Countryman,[105] P. Couvares,[1] P. B. Covas,[101] E. E. Cowan,[77] D. M. Coward,[65] M. J. Cowart,[7] D. C. Coyne,[1] R. Coyne,[107] J. D. E. Creighton,[24] T. D. Creighton,[108] J. Cripe,[2] M. Croquette,[72] S. G. Crowder,[109] T. J. Cullen,[2] A. Cumming,[45] L. Cunningham,[45] E. Cuoco,[29] T. Dal Canton,[80] G. Dálya,[110] B. D'Angelo,[81,58] S. L. Danilishin,[9,10] S. D'Antonio,[31] K. Danzmann,[10,9] A. Dasgupta,[111] C. F. Da Silva Costa,[30] L. E. H. Datrier,[45] V. Dattilo,[29] I. Dave,[59] M. Davier,[28] D. Davis,[41] E. J. Daw,[112] D. DeBra,[50] M. Deenadayalan,[3] J. Degallaix,[23] M. De Laurentis,[79,5] S. Déléglise,[72] W. Del Pozzo,[20,21] L. M. DeMarchi,[57] N. Demos,[14] T. Dent,[113] R. De Pietri,[114,115] R. De Rosa,[79,5] C. De Rossi,[23,29] R. DeSalvo,[116] O. de Varona,[9,10] S. Dhurandhar,[3] M. C. Díaz,[108] T. Dietrich,[36] L. Di Fiore,[5] C. DiFronzo,[13] C. Di Giorgio,[67,68] F. Di Giovanni,[22] M. Di Giovanni,[117,118] T. Di Girolamo,[79,5] A. Di Lieto,[20,21] B. Ding,[102] S. Di Pace,[119,32] I. Di Palma,[119,32] F. Di Renzo,[20,21] A. K. Divakarla,[30] A. Dmitriev,[13] Z. Doctor,[93] F. Donovan,[14] K. L. Dooley,[106,86] S. Doravari,[3] I. Dorrington,[106] T. P. Downes,[24] M. Drago,[16,17] J. C. Driggers,[46] Z. Du,[83] J.-G. Ducoin,[28] P. Dupej,[45] O. Durante,[67,68] S. E. Dwyer,[46] P. J. Easter,[6] G. Eddolls,[45] T. B. Edo,[112] A. Effler,[7] P. Ehrens,[1] J. Eichholz,[8] S. S. Eikenberry,[30] M. Eisenmann,[33] R. A. Eisenstein,[14] L. Errico,[79,5] R. C. Essick,[93] H. Estelles,[101] D. Estevez,[33] Z. B. Etienne,[38] T. Etzel,[1] M. Evans,[14] T. M. Evans,[7] V. Fafone,[85,31,16] S. Fairhurst,[106] X. Fan,[83] S. Farinon,[58] B. Farr,[71] W. M. Farr,[13] E. J. Fauchon-Jones,[106] M. Favata,[35] M. Fays,[112] M. Fazio,[120] C. Fee,[121] J. Feicht,[1] M. M. Fejer,[50] F. Feng,[26] A. Fernandez-Galiana,[14] I. Ferrante,[20,21] E. C. Ferreira,[15] T. A. Ferreira,[15] F. Fidecaro,[20,21] I. Fiori,[29] D. Fiorucci,[16,17] M. Fishbach,[93] R. P. Fisher,[122] J. M. Fishner,[14] R. Fittipaldi,[123,68] M. Fitz-Axen,[42] V. Fiumara,[124,68] R. Flaminio,[33,125] M. Fletcher,[45] E. Floden,[42] E. Flynn,[27] H. Fong,[82] J. A. Font,[22,126] P. W. F. Forsyth,[8] J.-D. Fournier,[64] Francisco Hernandez Vivanco,[6] S. Frasca,[119,32] F. Frasconi,[21] Z. Frei,[110] A. Freise,[13] R. Frey,[71] V. Frey,[28] P. Fritschel,[14] V. V. Frolov,[7] G. Fronzè,[127] P. Fulda,[30] M. Fyffe,[7] H. A. Gabbard,[45] B. U. Gadre,[75] S. M. Gaebel,[13] J. R. Gair,[128] L. Gammaitoni,[39] S. G. Gaonkar,[3] C. García-Quirós,[101] F. Garufi,[79,5] B. Gateley,[46] S. Gaudio,[34] G. Gaur,[129] V. Gayathri,[130] G. Gemme,[58] E. Genin,[29] A. Gennai,[21] D. George,[19] J. George,[59] L. Gergely,[131] S. Ghonge,[77] Abhirup Ghosh,[75] Archisman Ghosh,[36] S. Ghosh,[24] B. Giacomazzo,[117,118] J. A. Giaime,[2,7] K. D. Giardina,[7] D. R. Gibson,[132] K. Gill,[105]

L. Glover,[133] J. Gniesmer,[134] P. Godwin,[89] E. Goetz,[46] R. Goetz,[30] B. Goncharov,[6] G. González,[2] J. M. Gonzalez Castro,[20,21] A. Gopakumar,[135] S. E. Gossan,[1] M. Gosselin,[29,20,21] R. Gouaty,[33] B. Grace,[8] A. Grado,[136,5] M. Granata,[23] A. Grant,[45] S. Gras,[14] P. Grassia,[1] C. Gray,[46] R. Gray,[45] G. Greco,[62,63] A. C. Green,[30] R. Green,[106] E. M. Gretarsson,[34] A. Grimaldi,[117,118] S. J. Grimm,[16,17] P. Groot,[66] H. Grote,[106] S. Grunewald,[75] P. Gruning,[28] G. M. Guidi,[62,63] H. K. Gulati,[111] Y. Guo,[36] A. Gupta,[89] Anchal Gupta,[1] P. Gupta,[36] E. K. Gustafson,[1] R. Gustafson,[137] L. Haegel,[101] O. Halim,[17,16] B. R. Hall,[138] E. D. Hall,[14] E. Z. Hamilton,[106] G. Hammond,[45] M. Haney,[69] M. M. Hanke,[9,10] J. Hanks,[46] C. Hanna,[89] M. D. Hannam,[106] O. A. Hannuksela,[94] T. J. Hansen,[34] J. Hanson,[7] T. Harder,[64] T. Hardwick,[2] K. Haris,[18] J. Harms,[16,17] G. M. Harry,[139] I. W. Harry,[140] R. K. Hasskew,[7] C. J. Haster,[14] K. Haughian,[45] F. J. Hayes,[45] J. Healy,[61] A. Heidmann,[72] M. C. Heintze,[7] H. Heitmann,[64] F. Hellman,[141] P. Hello,[28] G. Hemming,[29] M. Hendry,[45] I. S. Heng,[45] J. Hennig,[9,10] M. Heurs,[9,10] S. Hild,[45] T. Hinderer,[142,36,143] S. Hochheim,[9,10] D. Hofman,[23] A. M. Holgado,[19] N. A. Holland,[8] K. Holt,[7] D. E. Holz,[93] P. Hopkins,[106] C. Horst,[24] J. Hough,[45] E. J. Howell,[65] C. G. Hoy,[106] Y. Huang,[14] M. T. Hübner,[6] E. A. Huerta,[19] D. Huet,[28] B. Hughey,[34] V. Hui,[33] S. Husa,[101] S. H. Huttner,[45] T. Huynh-Dinh,[7] B. Idzkowski,[73] A. Iess,[85,31] H. Inchauspe,[30] C. Ingram,[56] R. Inta,[84] G. Intini,[119,32] B. Irwin,[121] H. N. Isa,[45] J.-M. Isac,[72] M. Isi,[14] B. R. Iyer,[18] T. Jacqmin,[72] S. J. Jadhav,[144] K. Jani,[77] N. N. Janthalur,[144] P. Jaranowski,[145] D. Jariwala,[30] A. C. Jenkins,[146] J. Jiang,[30] D. S. Johnson,[19] A. W. Jones,[13] D. I. Jones,[147] J. D. Jones,[46] R. Jones,[45] R. J. G. Jonker,[36] L. Ju,[65] J. Junker,[9,10] C. V. Kalaghatgi,[106] V. Kalogera,[57] B. Kamai,[1] S. Kandhasamy,[3] G. Kang,[37] J. B. Kanner,[1] S. J. Kapadia,[24] S. Karki,[71] R. Kashyap,[18] M. Kasprzack,[1] S. Katsanevas,[29] E. Katsavounidis,[14] W. Katzman,[7] S. Kaufer,[10] K. Kawabe,[46] N. V. Keerthana,[3] F. Kéfélian,[64] D. Keitel,[140] R. Kennedy,[112] J. S. Key,[148] F. Y. Khalili,[60] I. Khan,[16,31] S. Khan,[9,10] E. A. Khazanov,[149] N. Khetan,[16,17] M. Khursheed,[59] N. Kijbunchoo,[8] Chunglee Kim,[150] J. C. Kim,[151] K. Kim,[94] W. Kim,[56] W. S. Kim,[152] Y.-M. Kim,[153] C. Kimball,[57] P. J. King,[46] M. Kinley-Hanlon,[45] R. Kirchhoff,[9,10] J. S. Kissel,[46] L. Kleybolte,[134] J. H. Klika,[24] S. Klimenko,[30] T. D. Knowles,[38] P. Koch,[9,10] S. M. Koehlenbeck,[9,10] G. Koekoek,[36,154] S. Koley,[36] V. Kondrashov,[1] A. Kontos,[155] N. Koper,[9,10] M. Korobko,[134] W. Z. Korth,[1] M. Kovalam,[65] D. B. Kozak,[1] C. Krämer,[9,10] V. Kringel,[9,10] N. Krishnendu,[156] A. Królak,[157,158] N. Krupinski,[24] G. Kuehn,[9,10] A. Kumar,[144] P. Kumar,[159] Rahul Kumar,[46] Rakesh Kumar,[111] L. Kuo,[90] A. Kutynia,[157] S. Kwang,[24] B. D. Lackey,[75] D. Laghi,[20,21] K. H. Lai,[94] T. L. Lam,[94] M. Landry,[46] B. B. Lane,[14] R. N. Lang,[160] J. Lange,[61] B. Lantz,[50] R. K. Lanza,[14] A. Lartaux-Vollard,[28] P. D. Lasky,[6] M. Laxen,[7] A. Lazzarini,[1] C. Lazzaro,[53] P. Leaci,[119,32] S. Leavey,[9,10] Y. K. Lecoeuche,[46] C. H. Lee,[97] H. K. Lee,[161] H. M. Lee,[162] H. W. Lee,[151] J. Lee,[96] K. Lee,[45] J. Lehmann,[9,10] A. K. Lenon,[38] N. Leroy,[28] N. Letendre,[33] Y. Levin,[6] A. Li,[94] J. Li,[83] K. J. L. Li,[94] T. G. F. Li,[94] X. Li,[47] F. Lin,[6] F. Linde,[163,36] S. D. Linker,[133] T. B. Littenberg,[164] J. Liu,[65] X. Liu,[24] M. Llorens-Monteagudo,[22] R. K. L. Lo,[94,1] L. T. London,[14] A. Longo,[165,166] M. Lorenzini,[16,17] V. Loriette,[167] M. Lormand,[7] G. Losurdo,[21] J. D. Lough,[9,10] C. O. Lousto,[61] G. Lovelace,[27] M. E. Lower,[168] H. Lück,[10,9] D. Lumaca,[85,31] A. P. Lundgren,[140] R. Lynch,[14] Y. Ma,[47] R. Macas,[106] S. Macfoy,[25] M. MacInnis,[14] D. M. Macleod,[106] A. Macquet,[64] I. Magaña Hernandez,[24] F. Magaña-Sandoval,[30] R. M. Magee,[89] E. Majorana,[32] I. Maksimovic,[167] A. Malik,[59] N. Man,[64] V. Mandic,[42] V. Mangano,[45,119,32] G. L. Mansell,[46,14] M. Manske,[24] M. Mantovani,[29] M. Mapelli,[52,53] F. Marchesoni,[51,40] F. Marion,[33] S. Márka,[105] Z. Márka,[105] C. Markakis,[19] A. S. Markosyan,[50] A. Markowitz,[1] E. Maros,[1] A. Marquina,[104] S. Marsat,[26] F. Martelli,[62,63] I. W. Martin,[45] R. M. Martin,[35] V. Martinez,[78] D. V. Martynov,[13] H. Masalehdan,[134] K. Mason,[14] E. Massera,[112] A. Masserot,[33] T. J. Massinger,[1] M. Masso-Reid,[45] S. Mastrogiovanni,[26] A. Matas,[75] F. Matichard,[1,14] L. Matone,[105] N. Mavalvala,[14] J. J. McCann,[65] R. McCarthy,[46] D. E. McClelland,[8] S. McCormick,[7] L. McCuller,[14] S. C. McGuire,[169] C. McIsaac,[140] J. McIver,[1] D. J. McManus,[8] T. McRae,[8] S. T. McWilliams,[38] D. Meacher,[24] G. D. Meadors,[6] M. Mehmet,[9,10] A. K. Mehta,[18] J. Meidam,[36] E. Mejuto Villa,[116,68] A. Melatos,[100] G. Mendell,[46] R. A. Mercer,[24] L. Mereni,[23] K. Merfeld,[71] E. L. Merilh,[46] M. Merzougui,[64] S. Meshkov,[1] C. Messenger,[45] C. Messick,[89] F. Messina,[43,44] R. Metzdorff,[72] P. M. Meyers,[100] F. Meylahn,[9,10] A. Miani,[117,118] H. Miao,[13] C. Michel,[23] H. Middleton,[100] L. Milano,[79,5] A. L. Miller,[30,119,32] M. Millhouse,[100] J. C. Mills,[106] M. C. Milovich-Goff,[133] O. Minazzoli,[64,170] Y. Minenkov,[31] A. Mishkin,[30] C. Mishra,[171] T. Mistry,[112] S. Mitra,[3] V. P. Mitrofanov,[60] G. Mitselmakher,[30] R. Mittleman,[14] G. Mo,[98] D. Moffa,[121] K. Mogushi,[86] S. R. P. Mohapatra,[14] M. Molina-Ruiz,[141] M. Mondin,[133] M. Montani,[62,63] C. J. Moore,[13] D. Moraru,[46] F. Morawski,[55] G. Moreno,[46] S. Morisaki,[82] B. Mours,[33] C. M. Mow-Lowry,[13] F. Muciaccia,[119,32] Arunava Mukherjee,[9,10] D. Mukherjee,[24] S. Mukherjee,[108] Subroto Mukherjee,[111] N. Mukund,[9,10,3] A. Mullavey,[7] J. Munch,[56] E. A. Muñiz,[41] M. Muratore,[34] P. G. Murray,[45] A. Nagar,[88,127,172] I. Nardecchia,[85,31] L. Naticchioni,[119,32] R. K. Nayak,[173] B. F. Neil,[65] J. Neilson,[116,68] G. Nelemans,[66,36] T. J. N. Nelson,[7] M. Nery,[9,10] A. Neunzert,[137] L. Nevin,[1] K. Y. Ng,[14] S. Ng,[56] C. Nguyen,[26] P. Nguyen,[71] D. Nichols,[142,36] S. A. Nichols,[2] S. Nissanke,[142,36] F. Nocera,[29] C. North,[106] L. K. Nuttall,[140] M. Obergaulinger,[22,174]

J. Oberling,[46] B. D. O'Brien,[30] G. Oganesyan,[16,17] G. H. Ogin,[175] J. J. Oh,[152] S. H. Oh,[152] F. Ohme,[9,10] H. Ohta,[82] M. A. Okada,[15] M. Oliver,[101] P. Oppermann,[9,10] Richard J. Oram,[7] B. O'Reilly,[7] R. G. Ormiston,[42] L. F. Ortega,[30] R. O'Shaughnessy,[61] S. Ossokine,[75] D. J. Ottaway,[56] H. Overmier,[7] B. J. Owen,[84] A. E. Pace,[89] G. Pagano,[20,21] M. A. Page,[65] G. Pagliaroli,[16,17] A. Pai,[130] S. A. Pai,[59] J. R. Palamos,[71] O. Palashov,[149] C. Palomba,[32] H. Pan,[90] P. K. Panda,[144] P. T. H. Pang,[94,36] C. Pankow,[57] F. Pannarale,[119,32] B. C. Pant,[59] F. Paoletti,[21] A. Paoli,[29] A. Parida,[3] W. Parker,[7,169] D. Pascucci,[45,36] A. Pasqualetti,[29] R. Passaquieti,[20,21] D. Passuello,[21] M. Patil,[158] B. Patricelli,[20,21] E. Payne,[6] B. L. Pearlstone,[45] T. C. Pechsiri,[30] A. J. Pedersen,[41] M. Pedraza,[1] R. Pedurand,[23,176] A. Pele,[7] S. Penn,[177] A. Perego,[117,118] C. J. Perez,[46] C. Périgois,[33] A. Perreca,[117,118] J. Petermann,[134] H. P. Pfeiffer,[75] M. Phelps,[9,10] K. S. Phukon,[3] O. J. Piccinni,[119,32] M. Pichot,[64] F. Piergiovanni,[62,63] V. Pierro,[116,68] G. Pillant,[29] L. Pinard,[23] I. M. Pinto,[116,68,88] M. Pirello,[46] M. Pitkin,[45] W. Plastino,[165,166] R. Poggiani,[20,21] D. Y. T. Pong,[94] S. Ponrathnam,[3] P. Popolizio,[29] E. K. Porter,[26] J. Powell,[168] A. K. Prajapati,[111] J. Prasad,[3] K. Prasai,[50] R. Prasanna,[144] G. Pratten,[101] T. Prestegard,[24] M. Principe,[116,88,68] G. A. Prodi,[117,118] L. Prokhorov,[13] M. Punturo,[40] P. Puppo,[32] M. Pürrer,[75] H. Qi,[106] V. Quetschke,[108] P. J. Quinonez,[34] F. J. Raab,[46] G. Raaijmakers,[142,36] H. Radkins,[46] N. Radulesco,[64] P. Raffai,[110] S. Raja,[59] C. Rajan,[59] B. Rajbhandari,[84] M. Rakhmanov,[108] K. E. Ramirez,[108] A. Ramos-Buades,[101] Javed Rana,[3] K. Rao,[57] P. Rapagnani,[119,32] V. Raymond,[106] M. Razzano,[20,21] J. Read,[27] T. Regimbau,[33] L. Rei,[58] S. Reid,[25] D. H. Reitze,[1,30] P. Rettegno,[127,178] F. Ricci,[119,32] C. J. Richardson,[34] J. W. Richardson,[1] P. M. Ricker,[19] G. Riemenschneider,[178,127] K. Riles,[137] M. Rizzo,[57] N. A. Robertson,[1,45] F. Robinet,[28] A. Rocchi,[31] L. Rolland,[33] J. G. Rollins,[1] V. J. Roma,[71] M. Romanelli,[70] R. Romano,[4,5] C. L. Romel,[46] J. H. Romie,[7] C. A. Rose,[24] D. Rose,[27] K. Rose,[121] D. Rosińska,[73] S. G. Rosofsky,[19] M. P. Ross,[179] S. Rowan,[45] A. Rüdiger,[9,10,*] P. Ruggi,[29] G. Rutins,[132] K. Ryan,[46] S. Sachdev,[89] T. Sadecki,[46] M. Sakellariadou,[146] O. S. Salafia,[180,43,44] L. Salconi,[29] M. Saleem,[156] A. Samajdar,[36] L. Sammut,[6] E. J. Sanchez,[1] L. E. Sanchez,[1] N. Sanchis-Gual,[181] J. R. Sanders,[182] K. A. Santiago,[35] E. Santos,[64] N. Sarin,[6] B. Sassolas,[23,106] O. Sauter,[137,33] R. L. Savage,[46] P. Schale,[71] M. Scheel,[47] J. Scheuer,[57] P. Schmidt,[13,66] R. Schnabel,[134] R. M. S. Schofield,[71] A. Schönbeck,[134] E. Schreiber,[9,10] B. W. Schulte,[9,10] B. F. Schutz,[106] J. Scott,[45] S. M. Scott,[8] E. Seidel,[19] D. Sellers,[7] A. S. Sengupta,[183] N. Sennett,[75] D. Sentenac,[29] V. Sequino,[58] A. Sergeev,[149] Y. Setyawati,[9,10] D. A. Shaddock,[8] T. Shaffer,[46] M. S. Shahriar,[57] M. B. Shaner,[133] A. Sharma,[16,17] P. Sharma,[59] P. Shawhan,[76] H. Shen,[19] R. Shink,[184] D. H. Shoemaker,[14] D. M. Shoemaker,[77] K. Shukla,[141] S. ShyamSundar,[59] K. Siellez,[77] M. Sieniawska,[55] D. Sigg,[46] L. P. Singer,[80] D. Singh,[89] N. Singh,[73] A. Singhal,[16,32] A. M. Sintes,[101] S. Sitmukhambetov,[108] V. Skliris,[106] B. J. J. Slagmolen,[8] T. J. Slaven-Blair,[65] J. R. Smith,[27] R. J. E. Smith,[6] S. Somala,[185] E. J. Son,[152] S. Soni,[2] B. Sorazu,[45] F. Sorrentino,[58] T. Souradeep,[3] E. Sowell,[84] A. P. Spencer,[45] M. Spera,[52,53] A. K. Srivastava,[111] V. Srivastava,[41] K. Staats,[57] C. Stachie,[64] M. Standke,[9,10] D. A. Steer,[26] M. Steinke,[9,10] J. Steinlechner,[134,45] S. Steinlechner,[134] D. Steinmeyer,[9,10] S. P. Stevenson,[168] D. Stocks,[50] R. Stone,[108] D. J. Stops,[13] K. A. Strain,[45] G. Stratta,[186,63] S. E. Strigin,[60] A. Strunk,[46] R. Sturani,[187] A. L. Stuver,[188] V. Sudhir,[14] T. Z. Summerscales,[189] L. Sun,[1] S. Sunil,[111] A. Sur,[55] J. Suresh,[82] P. J. Sutton,[106] B. L. Swinkels,[36] M. J. Szczepańczyk,[34] M. Tacca,[36] S. C. Tait,[45] C. Talbot,[6] D. B. Tanner,[30] D. Tao,[1] M. Tápai,[131] A. Tapia,[27] J. D. Tasson,[98] R. Taylor,[1] R. Tenorio,[101] L. Terkowski,[134] M. Thomas,[7] P. Thomas,[46] S. R. Thondapu,[59] K. A. Thorne,[7] E. Thrane,[6] Shubhanshu Tiwari,[117,118] Srishti Tiwari,[135] V. Tiwari,[106] K. Toland,[45] M. Tonelli,[20,21] Z. Tornasi,[45] A. Torres-Forné,[190] C. I. Torrie,[1] D. Töyrä,[13] F. Travasso,[29,40] G. Traylor,[7] M. C. Tringali,[73] A. Tripathee,[137] A. Trovato,[26] L. Trozzo,[191,21] K. W. Tsang,[36] M. Tse,[14] R. Tso,[47] L. Tsukada,[82] D. Tsuna,[82] T. Tsutsui,[82] D. Tuyenbayev,[108] K. Ueno,[82] D. Ugolini,[192] C. S. Unnikrishnan,[135] A. L. Urban,[2] S. A. Usman,[93] H. Vahlbruch,[10] G. Vajente,[1] G. Valdes,[2] M. Valentini,[117,118] N. van Bakel,[36] M. van Beuzekom,[36] J. F. J. van den Brand,[74,36] C. Van Den Broeck,[36,193] D. C. Vander-Hyde,[41] L. van der Schaaf,[36] J. V. VanHeijningen,[65] A. A. van Veggel,[45] M. Vardaro,[52,53] V. Varma,[47] S. Vass,[1] M. Vasúth,[49] A. Vecchio,[13] G. Vedovato,[53] J. Veitch,[45] P. J. Veitch,[56] K. Venkateswara,[179] G. Venugopalan,[1] D. Verkindt,[33] F. Vetrano,[62,63] A. Viceré,[62,63] A. D. Viets,[24] S. Vinciguerra,[13] D. J. Vine,[132] J.-Y. Vinet,[64] S. Vitale,[14] T. Vo,[41] H. Vocca,[39,40] C. Vorvick,[46] S. P. Vyatchanin,[60] A. R. Wade,[1] L. E. Wade,[121] M. Wade,[121] R. Walet,[36] M. Walker,[27] L. Wallace,[1] S. Walsh,[24] H. Wang,[13] J. Z. Wang,[137] S. Wang,[19] W. H. Wang,[108] Y. F. Wang,[94] R. L. Ward,[8] Z. A. Warden,[34] J. Warner,[46] M. Was,[33] J. Watchi,[102] B. Weaver,[46] L.-W. Wei,[9,10] M. Weinert,[9,10] A. J. Weinstein,[1] R. Weiss,[14] F. Wellmann,[9,10] L. Wen,[65] E. K. Wessel,[19] P. Weßels,[9,10] J. W. Westhouse,[34] K. Wette,[8] J. T. Whelan,[61] B. F. Whiting,[30] C. Whittle,[14] D. M. Wilken,[9,10] D. Williams,[45] A. R. Williamson,[142,36] J. L. Willis,[1] B. Willke,[10,9] W. Winkler,[9,10] C. C. Wipf,[1] H. Wittel,[9,10] G. Woan,[45] J. Woehler,[9,10] J. K. Wofford,[61] J. L. Wright,[45] D. S. Wu,[9,10] D. M. Wysocki,[61] S. Xiao,[1] R. Xu,[109] H. Yamamoto,[1] C. C. Yancey,[76] L. Yang,[120] Y. Yang,[30] Z. Yang,[42] M. J. Yap,[8] M. Yazback,[30] D. W. Yeeles,[106] Hang Yu,[14] Haocun Yu,[14] S. H. R. Yuen,[94]

A. K. Zadrożny,[108] A. Zadrożny,[157] M. Zanolin,[34] T. Zelenova,[29] J.-P. Zendri,[53] M. Zevin,[57] J. Zhang,[65] L. Zhang,[1] T. Zhang,[45] C. Zhao,[65] G. Zhao,[102] M. Zhou,[57] Z. Zhou,[57] X. J. Zhu,[6] M. E. Zucker,[1,14] J. Zweizig,[1] M. A. Papa,[9,10,24] and F. Salemi[9]

(LIGO Scientific Collaboration and Virgo Collaboration)

[1]*LIGO, California Institute of Technology, Pasadena, California 91125, USA*
[2]*Louisiana State University, Baton Rouge, Louisiana 70803, USA*
[3]*Inter-University Centre for Astronomy and Astrophysics, Pune 411007, India*
[4]*Dipartimento di Farmacia, Università di Salerno, I-84084 Fisciano, Salerno, Italy*
[5]*INFN, Sezione di Napoli, Complesso Universitario di Monte S.Angelo, I-80126 Napoli, Italy*
[6]*OzGrav, School of Physics & Astronomy, Monash University, Clayton 3800, Victoria, Australia*
[7]*LIGO Livingston Observatory, Livingston, Louisiana 70754, USA*
[8]*OzGrav, Australian National University, Canberra, Australian Capital Territory 0200, Australia*
[9]*Max Planck Institute for Gravitational Physics (Albert Einstein Institute), D-30167 Hannover, Germany*
[10]*Leibniz Universität Hannover, D-30167 Hannover, Germany*
[11]*Theoretisch-Physikalisches Institut, Friedrich-Schiller-Universität Jena, D-07743 Jena, Germany*
[12]*University of Cambridge, Cambridge CB2 1TN, United Kingdom*
[13]*University of Birmingham, Birmingham B15 2TT, United Kingdom*
[14]*LIGO, Massachusetts Institute of Technology, Cambridge, Massachusetts 02139, USA*
[15]*Instituto Nacional de Pesquisas Espaciais, 12227-010 São José dos Campos, São Paulo, Brazil*
[16]*Gran Sasso Science Institute (GSSI), I-67100 L'Aquila, Italy*
[17]*INFN, Laboratori Nazionali del Gran Sasso, I-67100 Assergi, Italy*
[18]*International Centre for Theoretical Sciences, Tata Institute of Fundamental Research,
Bengaluru 560089, India*
[19]*NCSA, University of Illinois at Urbana-Champaign, Urbana, Illinois 61801, USA*
[20]*Università di Pisa, I-56127 Pisa, Italy*
[21]*INFN, Sezione di Pisa, I-56127 Pisa, Italy*
[22]*Departamento de Astronomía y Astrofísica, Universitat de València, E-46100 Burjassot, València, Spain*
[23]*Laboratoire des Matériaux Avancés (LMA), CNRS/IN2P3, F-69622 Villeurbanne, France*
[24]*University of Wisconsin-Milwaukee, Milwaukee, Wisconsin 53201, USA*
[25]*SUPA, University of Strathclyde, Glasgow G1 1XQ, United Kingdom*
[26]*APC, AstroParticule et Cosmologie, Université Paris Diderot, CNRS/IN2P3, CEA/Irfu, Observatoire de
Paris, Sorbonne Paris Cité, F-75205 Paris Cedex 13, France*
[27]*California State University Fullerton, Fullerton, California 92831, USA*
[28]*LAL, Univ. Paris-Sud, CNRS/IN2P3, Université Paris-Saclay, F-91898 Orsay, France*
[29]*European Gravitational Observatory (EGO), I-56021 Cascina, Pisa, Italy*
[30]*University of Florida, Gainesville, Florida 32611, USA*
[31]*INFN, Sezione di Roma Tor Vergata, I-00133 Roma, Italy*
[32]*INFN, Sezione di Roma, I-00185 Roma, Italy*
[33]*Laboratoire d'Annecy de Physique des Particules (LAPP), Univ. Grenoble Alpes, Université Savoie
Mont Blanc, CNRS/IN2P3, F-74941 Annecy, France*
[34]*Embry-Riddle Aeronautical University, Prescott, Arizona 86301, USA*
[35]*Montclair State University, Montclair, New Jersey 07043, USA*
[36]*Nikhef, Science Park 105, 1098 XG Amsterdam, Netherlands*
[37]*Korea Institute of Science and Technology Information, Daejeon 34141, South Korea*
[38]*West Virginia University, Morgantown, West Virginia 26506, USA*
[39]*Università di Perugia, I-06123 Perugia, Italy*
[40]*INFN, Sezione di Perugia, I-06123 Perugia, Italy*
[41]*Syracuse University, Syracuse, New York 13244, USA*
[42]*University of Minnesota, Minneapolis, Minnesota 55455, USA*
[43]*Università degli Studi di Milano-Bicocca, I-20126 Milano, Italy*
[44]*INFN, Sezione di Milano-Bicocca, I-20126 Milano, Italy*
[45]*SUPA, University of Glasgow, Glasgow G12 8QQ, United Kingdom*
[46]*LIGO Hanford Observatory, Richland, Washington 99352, USA*
[47]*Caltech CaRT, Pasadena, California 91125, USA*
[48]*Dipartimento di Medicina, Chirurgia e Odontoiatria "Scuola Medica Salernitana,"
Università di Salerno, I-84081 Baronissi, Salerno, Italy*
[49]*Wigner RCP, RMKI, H-1121 Budapest, Konkoly Thege Miklós út 29-33, Hungary*

[50]*Stanford University, Stanford, California 94305, USA*

[51]*Università di Camerino, Dipartimento di Fisica, I-62032 Camerino, Italy*

[52]*Università di Padova, Dipartimento di Fisica e Astronomia, I-35131 Padova, Italy*

[53]*INFN, Sezione di Padova, I-35131 Padova, Italy*

[54]*Montana State University, Bozeman, Montana 59717, USA*

[55]*Nicolaus Copernicus Astronomical Center, Polish Academy of Sciences, 00-716, Warsaw, Poland*

[56]*OzGrav, University of Adelaide, Adelaide, South Australia 5005, Australia*

[57]*Center for Interdisciplinary Exploration & Research in Astrophysics (CIERA), Northwestern University, Evanston, Illinois 60208, USA*

[58]*INFN, Sezione di Genova, I-16146 Genova, Italy*

[59]*RRCAT, Indore, Madhya Pradesh 452013, India*

[60]*Faculty of Physics, Lomonosov Moscow State University, Moscow 119991, Russia*

[61]*Rochester Institute of Technology, Rochester, New York 14623, USA*

[62]*Università degli Studi di Urbino "Carlo Bo," I-61029 Urbino, Italy*

[63]*INFN, Sezione di Firenze, I-50019 Sesto Fiorentino, Firenze, Italy*

[64]*Artemis, Université Côte d'Azur, Observatoire Côte d'Azur, CNRS, CS 34229, F-06304 Nice Cedex 4, France*

[65]*OzGrav, University of Western Australia, Crawley, Western Australia 6009, Australia*

[66]*Department of Astrophysics/IMAPP, Radboud University Nijmegen, P.O. Box 9010, 6500 GL Nijmegen, Netherlands*

[67]*Dipartimento di Fisica "E.R. Caianiello," Università di Salerno, I-84084 Fisciano, Salerno, Italy*

[68]*INFN, Sezione di Napoli, Gruppo Collegato di Salerno, Complesso Universitario di Monte S. Angelo, I-80126 Napoli, Italy*

[69]*Physik-Institut, University of Zurich, Winterthurerstrasse 190, 8057 Zurich, Switzerland*

[70]*Univ Rennes, CNRS, Institut FOTON-UMR6082, F-3500 Rennes, France*

[71]*University of Oregon, Eugene, Oregon 97403, USA*

[72]*Laboratoire Kastler Brossel, Sorbonne Université, CNRS, ENS-Université PSL, Collège de France, F-75005 Paris, France*

[73]*Astronomical Observatory Warsaw University, 00-478 Warsaw, Poland*

[74]*VU University Amsterdam, 1081 HV Amsterdam, Netherlands*

[75]*Max Planck Institute for Gravitational Physics (Albert Einstein Institute), D-14476 Potsdam-Golm, Germany*

[76]*University of Maryland, College Park, Maryland 20742, USA*

[77]*School of Physics, Georgia Institute of Technology, Atlanta, Georgia 30332, USA*

[78]*Université de Lyon, Université Claude Bernard Lyon 1, CNRS, Institut Lumière Matière, F-69622 Villeurbanne, France*

[79]*Università di Napoli "Federico II," Complesso Universitario di Monte S.Angelo, I-80126 Napoli, Italy*

[80]*NASA Goddard Space Flight Center, Greenbelt, Maryland 20771, USA*

[81]*Dipartimento di Fisica, Università degli Studi di Genova, I-16146 Genova, Italy*

[82]*RESCEU, University of Tokyo, Tokyo, 113-0033, Japan*

[83]*Tsinghua University, Beijing 100084, China*

[84]*Texas Tech University, Lubbock, Texas 79409, USA*

[85]*Università di Roma Tor Vergata, I-00133 Roma, Italy*

[86]*The University of Mississippi, University, Mississippi 38677, USA*

[87]*Missouri University of Science and Technology, Rolla, Missouri 65409, USA*

[88]*Museo Storico della Fisica e Centro Studi e Ricerche "Enrico Fermi," I-00184 Roma, Italy*

[89]*The Pennsylvania State University, University Park, Pennsylvania 16802, USA*

[90]*National Tsing Hua University, Hsinchu City, 30013 Taiwan, Republic of China*

[91]*Charles Sturt University, Wagga Wagga, New South Wales 2678, Australia*

[92]*Canadian Institute for Theoretical Astrophysics, University of Toronto, Toronto, Ontario M5S 3H8, Canada*

[93]*University of Chicago, Chicago, Illinois 60637, USA*

[94]*The Chinese University of Hong Kong, Shatin, NT, Hong Kong*

[95]*Dipartimento di Ingegneria Industriale (DIIN), Università di Salerno, I-84084 Fisciano, Salerno, Italy*

[96]*Seoul National University, Seoul 08826, South Korea*

[97]*Pusan National University, Busan 46241, South Korea*

[98]*Carleton College, Northfield, Minnesota 55057, USA*

[99]*INAF, Osservatorio Astronomico di Padova, I-35122 Padova, Italy*

[100]*OzGrav, University of Melbourne, Parkville, Victoria 3010, Australia*

[101]*Universitat de les Illes Balears, IAC3—IEEC, E-07122 Palma de Mallorca, Spain*

[102]*Université Libre de Bruxelles, Brussels 1050, Belgium*

[103]*Sonoma State University, Rohnert Park, California 94928, USA*

[104]*Departamento de Matemáticas, Universitat de València, E-46100 Burjassot, València, Spain*

[105]*Columbia University, New York, New York 10027, USA*

[106]*Cardiff University, Cardiff CF24 3AA, United Kingdom*

[107]*University of Rhode Island, Kingston, Rhode Island 02881, USA*

[108]*The University of Texas Rio Grande Valley, Brownsville, Texas 78520, USA*

[109]*Bellevue College, Bellevue, Washington 98007, USA*

[110]*MTA-ELTE Astrophysics Research Group, Institute of Physics, Eötvös University, Budapest 1117, Hungary*

[111]*Institute for Plasma Research, Bhat, Gandhinagar 382428, India*

[112]*The University of Sheffield, Sheffield S10 2TN, United Kingdom*

[113]*IGFAE, Campus Sur, Universidade de Santiago de Compostela, 15782, Spain*

[114]*Dipartimento di Scienze Matematiche, Fisiche e Informatiche, Università di Parma, I-43124 Parma, Italy*

[115]*INFN, Sezione di Milano Bicocca, Gruppo Collegato di Parma, I-43124 Parma, Italy*

[116]*Dipartimento di Ingegneria, Università del Sannio, I-82100 Benevento, Italy*

[117]*Università di Trento, Dipartimento di Fisica, I-38123 Povo, Trento, Italy*

[118]*INFN, Trento Institute for Fundamental Physics and Applications, I-38123 Povo, Trento, Italy*

[119]*Università di Roma "La Sapienza," I-00185 Roma, Italy*

[120]*Colorado State University, Fort Collins, Colorado 80523, USA*

[121]*Kenyon College, Gambier, Ohio 43022, USA*

[122]*Christopher Newport University, Newport News, Virginia 23606, USA*

[123]*CNR-SPIN, c/o Università di Salerno, I-84084 Fisciano, Salerno, Italy*

[124]*Scuola di Ingegneria, Università della Basilicata, I-85100 Potenza, Italy*

[125]*National Astronomical Observatory of Japan, 2-21-1 Osawa, Mitaka, Tokyo 181-8588, Japan*

[126]*Observatori Astronòmic, Universitat de València, E-46980 Paterna, València, Spain*

[127]*INFN Sezione di Torino, I-10125 Torino, Italy*

[128]*School of Mathematics, University of Edinburgh, Edinburgh EH9 3FD, United Kingdom*

[129]*Institute Of Advanced Research, Gandhinagar 382426, India*

[130]*Indian Institute of Technology Bombay, Powai, Mumbai 400 076, India*

[131]*University of Szeged, Dóm tér 9, Szeged 6720, Hungary*

[132]*SUPA, University of the West of Scotland, Paisley PA1 2BE, United Kingdom*

[133]*California State University, Los Angeles, 5151 State University Dr, Los Angeles, California 90032, USA*

[134]*Universität Hamburg, D-22761 Hamburg, Germany*

[135]*Tata Institute of Fundamental Research, Mumbai 400005, India*

[136]*INAF, Osservatorio Astronomico di Capodimonte, I-80131 Napoli, Italy*

[137]*University of Michigan, Ann Arbor, Michigan 48109, USA*

[138]*Washington State University, Pullman, Washington 99164, USA*

[139]*American University, Washington, D.C. 20016, USA*

[140]*University of Portsmouth, Portsmouth, PO1 3FX, United Kingdom*

[141]*University of California, Berkeley, California 94720, USA*

[142]*GRAPPA, Anton Pannekoek Institute for Astronomy and Institute for High-Energy Physics, University of Amsterdam, Science Park 904, 1098 XH Amsterdam, Netherlands*

[143]*Delta Institute for Theoretical Physics, Science Park 904, 1090 GL Amsterdam, Netherlands*

[144]*Directorate of Construction, Services & Estate Management, Mumbai 400094 India*

[145]*University of Białystok, 15-424 Białystok, Poland*

[146]*King's College London, University of London, London WC2R 2LS, United Kingdom*

[147]*University of Southampton, Southampton SO17 1BJ, United Kingdom*

[148]*University of Washington Bothell, Bothell, Washington 98011, USA*

[149]*Institute of Applied Physics, Nizhny Novgorod, 603950, Russia*

[150]*Ewha Womans University, Seoul 03760, South Korea*

[151]*Inje University Gimhae, South Gyeongsang 50834, South Korea*

[152]*National Institute for Mathematical Sciences, Daejeon 34047, South Korea*

[153]*Ulsan National Institute of Science and Technology, Ulsan 44919, South Korea*

[154]*Maastricht University, P.O. Box 616, 6200 MD Maastricht, Netherlands*

[155]*Bard College, 30 Campus Rd, Annandale-On-Hudson, New York 12504, USA*

[156]*Chennai Mathematical Institute, Chennai 603103, India*

[157]*NCBJ, 05-400 Świerk-Otwock, Poland*

[158]*Institute of Mathematics, Polish Academy of Sciences, 00656 Warsaw, Poland*

[159]*Cornell University, Ithaca, New York 14850, USA*
[160]*Hillsdale College, Hillsdale, Michigan 49242, USA*
[161]*Hanyang University, Seoul 04763, South Korea*
[162]*Korea Astronomy and Space Science Institute, Daejeon 34055, South Korea*
[163]*Institute for High-Energy Physics, University of Amsterdam,*
Science Park 904, 1098 XH Amsterdam, Netherlands
[164]*NASA Marshall Space Flight Center, Huntsville, Alabama 35811, USA*
[165]*Dipartimento di Matematica e Fisica, Università degli Studi Roma Tre, I-00146 Roma, Italy*
[166]*INFN, Sezione di Roma Tre, I-00146 Roma, Italy*
[167]*ESPCI, CNRS, F-75005 Paris, France*
[168]*OzGrav, Swinburne University of Technology, Hawthorn VIC 3122, Australia*
[169]*Southern University and A&M College, Baton Rouge, Louisiana 70813, USA*
[170]*Centre Scientifique de Monaco, 8 quai Antoine Ier, MC-98000, Monaco*
[171]*Indian Institute of Technology Madras, Chennai 600036, India*
[172]*Institut des Hautes Etudes Scientifiquesi, F-91440 Bures-sur-Yvette, France*
[173]*IISER-Kolkata, Mohanpur, West Bengal 741252, India*
[174]*Institut für Kernphysik, Theoriezentrum, 64289 Darmstadt, Germany*
[175]*Whitman College, 345 Boyer Avenue, Walla Walla, Washington 99362, USA*
[176]*Université de Lyon, F-69361 Lyon, France*
[177]*Hobart and William Smith Colleges, Geneva, New York 14456, USA*
[178]*Dipartimento di Fisica, Università degli Studi di Torino, I-10125 Torino, Italy*
[179]*University of Washington, Seattle, Washington 98195, USA*
[180]*INAF, Osservatorio Astronomico di Brera sede di Merate, I-23807 Merate, Lecco, Italy*
[181]*Centro de Astrofísica e Gravitação (CENTRA), Departamento de Física, Instituto Superior Técnico,*
Universidade de Lisboa, 1049-001 Lisboa, Portugal
[182]*Marquette University, 11420 W. Clybourn St., Milwaukee, Wisconsin 53233, USA*
[183]*Indian Institute of Technology, Gandhinagar Ahmedabad Gujarat 382424, India*
[184]*Université de Montréal/Polytechnique, Montreal, Quebec H3T 1J4, Canada*
[185]*Indian Institute of Technology Hyderabad, Sangareddy, Khandi, Telangana 502285, India*
[186]*INAF, Osservatorio di Astrofisica e Scienza dello Spazio, I-40129 Bologna, Italy*
[187]*International Institute of Physics, Universidade Federal do Rio Grande do Norte,*
Natal RN 59078-970, Brazil
[188]*Villanova University, 800 Lancaster Ave, Villanova, Pennsylvania 19085, USA*
[189]*Andrews University, Berrien Springs, Michigan 49104, USA*
[190]*Max Planck Institute for Gravitationalphysik (Albert Einstein Institute),*
D-14476 Potsdam-Golm, Germany
[191]*Università di Siena, I-53100 Siena, Italy*
[192]*Trinity University, San Antonio, Texas 78212, USA*
[193]*Van Swinderen Institute for Particle Physics and Gravity, University of Groningen,*
Nijenborgh 4, 9747 AG Groningen, Netherlands